



ACCELERATED BRIDGE CONSTRUCTION
UNIVERSITY TRANSPORTATION CENTER

ABC-UTC GUIDE FOR:

HIGH-SPEED RAIL BRIDGE SYSTEMS

September 2019

End Date: December 2020

Performing Institutions:

*Florida International University /
University of Washington /
University of Nevada, Reno*

Authors:

*Andrew Stephenson, Michelle Chang,
Priya Tripathi, Seung Jae Lee, John
Stanton, Mohamed Moustafa, and
Marc Eberhard*



Image: California High-Speed Rail Fresno River Viaduct

IOWA STATE
UNIVERSITY



University of Nevada, Reno



Civil and Environmental
Engineering



WASHINGTON



The UNIVERSITY of OKLAHOMA



ACKNOWLEDGMENTS

The research study resulting in development of this guideline was supported by the US Department of Transportation through the Accelerated Bridge Construction University Transportation Center (ABC-UTC).

DISCLAIMER

Authors assume no responsibility for the use of this document. The opinions, findings, or conclusions expressed in this article do not represent the opinion of the US Department of Transportation.



NOMENCLATURE

<i>ABC</i>	<i>Accelerated Bridge Construction</i>
<i>BART</i>	<i>Bay Area Rapid Transit</i>
<i>BDS</i>	<i>Bridge Design Specifications</i>
<i>BNSF</i>	<i>Burlington Northern Santa Fe</i>
<i>CAHSR</i>	<i>California High-Speed Rail Authority</i>
<i>CHSTP</i>	<i>California High-Speed Train Project</i>
<i>CIDH</i>	<i>Cast-In Drilled-Hole</i>
<i>CIP</i>	<i>Cast-In Place</i>
<i>CISS</i>	<i>Cast-in Steel-Shell</i>
<i>CP</i>	<i>Construction Package</i>
<i>CRB</i>	<i>California Rail Builders</i>
<i>CRTS</i>	<i>China Railway Track Network</i>
<i>CSDC</i>	<i>Caltrans Seismic Design Criteria</i>
<i>CWR</i>	<i>Continuous Welded Rail</i>
<i>FRA</i>	<i>Federal Railroad Administration</i>
<i>HDPE</i>	<i>High Density Polyethylene</i>
<i>MLTRP</i>	<i>Medium- To Long-Term Railway Plan</i>
<i>FYP</i>	<i>Five-Year Railway Planning Plans</i>
<i>PDL</i>	<i>Passenger Dedicated Line</i>
<i>CWR</i>	<i>Continuous Welded Rail</i>
<i>IRCT</i>	<i>Institute Of Railway Comprehensive Technology Of Japan</i>
<i>CRTS</i>	<i>China Railway Track System</i>
<i>CWR</i>	<i>Continuous Welded Rail</i>
<i>CRH</i>	<i>China Railway High-Speed</i>
<i>CFST</i>	<i>Concrete Filled Steel Tubes</i>
<i>SCC</i>	<i>Self-Compacting Concrete</i>
<i>SR</i>	<i>State Route</i>
<i>DOT</i>	<i>Department Of Transportation</i>
<i>HSLM</i>	<i>High Speed Load Model</i>
<i>HSR</i>	<i>High-Speed Rail</i>
<i>HST</i>	<i>High-Speed Train</i>
<i>LRFD</i>	<i>Load and Resistance Factor Design</i>
<i>MCE</i>	<i>Maximum Considered Earthquake</i>
<i>MSS</i>	<i>Movable Scaffolding System</i>
<i>OBE</i>	<i>Operating Basis Earthquake</i>
<i>PDL</i>	<i>Passenger Dedicated Lines</i>
<i>TCR</i>	<i>Texas Central Railway</i>
<i>THSR</i>	<i>Taiwan High Speed Rail</i>
<i>UIC</i>	<i>International Union of Railways</i>



1. HSR BRIDGE DESIGN SPECIFICATIONS AND SELECTION METHODS

High-speed railway (HSR) provides a fast and robust travel choice that enhances transport of people and goods, which may act as the national economy's main artery. Compared to conventional railways, HSR has more stringent structural and geotechnical requirements to minimize deformations and avoid excessive vibrations. Bridges are a key component of the HSR infrastructure because it can avoid the interruption of existing roadways and the occupation of land. Several foreign countries including Japan and China have developed a standard design for the HSR infrastructure which stands as a great design reference for future projects within the United States. There is a wide range of HSR superstructure types around the world from 30 m box girder bridges to over 1000 m suspension bridges. Early designs used simply-supported, deep, post-tensioned concrete box girders (Kang et al. 2018), but since then many other types have emerged (Yan et al. 2015). Table 1.1 provides a partial list of different bridge types for reference, sorted by the length of span.

Table 1.1 Partial list of international HSR bridges

Name	City/Locality	Country	Year	Main Span (m)	Materials	Type
WuFengShan Bridge	Zhenjiang	China	2020	1092	multiple	Suspension
TianXingZhou Bridge	Wuhan	China	2009	504	multiple	Cable Stay
Almonte Viaduct	Alcantara	Spain	2016	384	Concrete	Arch
DaShengGuan Bridge	Nanjing	China	2010	336	Steel	Arch
Sannai-Maruyama Bridge	Aomori	Japan	2008	150	Concrete	Extradosed
Leuven HSR Bridge	Leuven	Belgium	2002	117	Steel	Arch
Avignon Viaducts	Avignon	France	1999	100	Concrete	Haunched box girders
Meuse Viaduct	Lacroix-sur-Meuse	France	2005	52	Composite	Haunched twin girders
Archidona Viaduct	Archidona	Spain	2012	50	Composite	Haunched twin girders



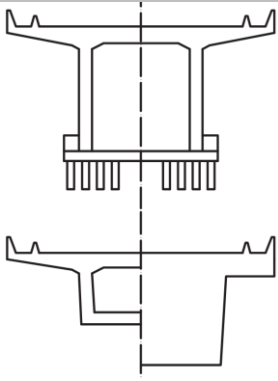
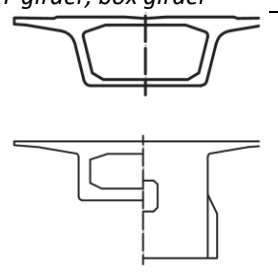
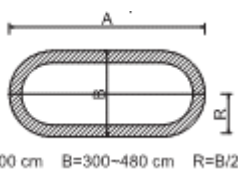
1.1. SUPERSTRUCTURE SYSTEMS

1.1.1. INTRODUCTION

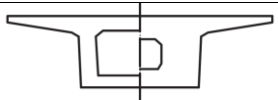
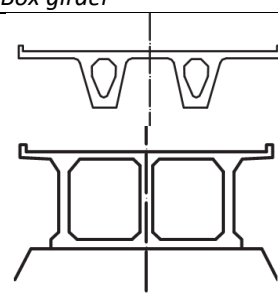
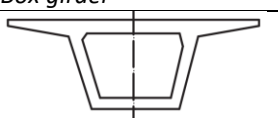
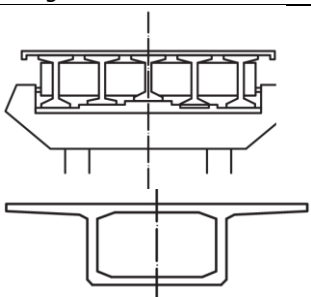
High-speed railway bridges are subject to complex vehicle loading and stringent serviceability criteria, which lead to structural solutions different from those used for highway bridges or conventional railway bridges. Due to the high speed of the trains, track deformations – and thus, structural deformations – must be kept to a minimum to limit excess acceleration and ensure passenger comfort. Additionally, vibrations and resonance are of concern.

This section provides a review of selected HSR design criteria from California, China, and Europe. These include the California High Speed Rail (CAHSR) Design Criteria, the Chinese Code for Design of High-Speed Railway, and Eurocode EN 1990 and EN 1992. Eurocode directly adapts the loads and limits recommended in UIC Leaflets 776-1R and 776-2R, while the California and Chinese criteria reference the UIC Leaflets as a guide, but do not follow UIC in some cases (Muncke 2008). Because the static and dynamic service load cases tend to govern the superstructure selection, special emphasis will be placed on service limits and the corresponding loads. Load cases and serviceability limits – including vertical deflection, rotation, acceleration, and natural frequency bounds – are discussed. The most common superstructure type for HSR is a simply supported pre-stressed concrete beam. Some features of simply supported beam bridges from six countries are listed in Table 1.2.

Table 1.2 Features of simply-supported HSR bridges from six countries (Yan et al. 2015)

Country	Typical Cross-Sections (L: at mid-span; R: at ends)	Standard Span(s)	Typical Pier and Foundation	Construction Method(s)
Japan	 T-girder, box girder	24.2, 29.2, 34.2, 39.2, and 44.2 m	Rectangular or circular pier Pile group or spread footing	Precast Cantilever Cast-in-place
China	 Box girder (2 types)	32 m	 A=800 cm B=300~480 cm R=B/2 Round-ended pier with pile group	Precast Cantilever



France	 Box girder	≤ 25 m	Rectangular or circular pier Pile group or spread footing	Precast Cantilever Cast-in-place
Italy	 Box girder	24, 33.6, 43.2, and 55.0 m	Rectangular pier Single pile	Cantilever Cast-in-place Launching
Germany	 Box girder	25, 44, and 58 m	Rectangular pier Single pile or pile group	Cast-in-place Launching
Spain	 I-girder or box girder	26.6 m	Rectangular pier Single pile or pile group	Cantilever

1.1.2. LOADING

The superimposed dead load of railway bridges is significantly larger than that of highway bridges due to the track structures (ballast, rail and fasteners, cables, poles, and walls). The live loads are also greater since railway vehicles, particularly the locomotives, are much heavier than typical highway vehicles. Additionally, horizontal forces imposed by trains – including acceleration, braking and centrifugal forces – are much larger than those from roadway vehicles. For example, braking forces can be up to 14 times greater in railway bridges than in highway bridges (Marx and Schlaich 2009), and centrifugal loads from trains can be 3-15 times those induced by highway traffic (Sobrino 2008). Furthermore, “nosing” and “hunting” forces (lateral forces that arise from random imperfections in the rails and wheels) occur in rail bridges but not highway bridges.

Also of key concern are the seismic loads on bridges where applicable. The CAHSR Design Criteria specify two levels of design earthquakes: An Operating Basis Earthquake (OBE) with a return period of 50 years, and a Maximum Considered Earthquake (MCE) with a return period of 950 years. This roughly corresponds with the Level 1 and Level 3 ground motion levels for conventional railway bridges, as described in the AREMA Manual for Railway Engineering. For HSR bridges in China, the earthquake loading is the same as those for Chinese conventional railway bridges, as

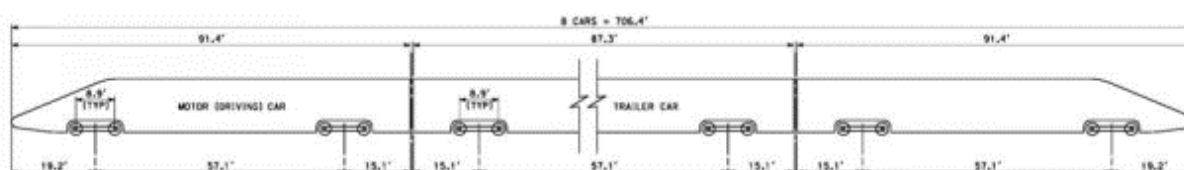


outlined in the Chinese Code for Seismic Design of Railway Engineering. There are three levels of earthquakes considered, with return periods of 50 years, 475 years, and 2475 years (labeled as the low, design, and high-level earthquakes, respectively).

While the aforementioned loads are to be considered in many analysis cases, the typical loads that control the superstructure type of HSR bridges tend to be the vertical live loads. In each country, there are several vertical live load patterns specified for HSR bridge design. These patterns may include a service HSR train load, or a heavier maintenance train load, which are applied in different permutations (e.g., one train on the bridge, two trains, etc.) in several analyses (e.g., static and dynamic track serviceability analysis, rail-structure interaction analysis, etc.). Some examples of service and maintenance train loads will be outlined here.

1.1.2.1. HIGH-SPEED TRAINS

California has yet to select the specific trainset to be used on the CAHSR system. Therefore, the CAHSR design specifications outline five trainsets to represent possible service loads. One trainset is shown in Figure 1.1.



Maximum Axle Load = 18.7 tons

Train Weight (Empty) = 509 tons

Figure 1.1. California Type 1 trainset (California High-Speed Rail Authority 2019)

Eurocode design specifications require that either the actual trains or the UIC High Speed Load Model (HSLM) are used for dynamic analyses. Because the high-speed trainsets may differ between countries, only the HSLM is described here.

The UIC HSLM represents the loading from passenger trains exceeding 200 km/h. There are two models within the HSLM. Both models are a series of point loads, but they differ in magnitude and spacing:

- HSLM-A consists of 10 trains. Analyses that require HSLM-A will indicate which of the 10 trains are to be used. The trains have varying numbers of train cars, axle spacing, and live load magnitude.
- HSLM-B is a series of equally spaced point loads, where the number of loads and their spacing is dependent on bridge span length.

Depending on the bridge configuration, HSLM-A or HSLM-B will be specified. Usually, only one track is loaded with a single train per case. For more information, see UIC 776-2R Section A.4.1.



1.1.2.2. MAINTENANCE AND CONVENTIONAL TRAINS

While the high-speed trains are more representative of actual service loads, many of the static serviceability limits are based off of maintenance or conventional rail trains. A sampling of trains is outlined here.

The CAHSR Design Criteria frequently use the Modified Cooper E-50 load shown in Figure 1.2. This is representative of a maintenance train for high-speed rail lines.

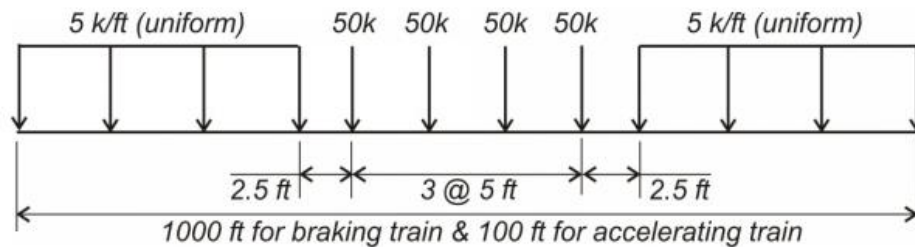


Figure 1.2. Modified Cooper E-50 load (California High-Speed Rail Authority 2019)

Eurocode references the UIC71 load shown in Figure 1.3. This load model is commonly used as a service train in conventional rail bridge design, but it is also used in high-speed rail design. It is similar in magnitude and distribution to the Modified Cooper E-50 loading.

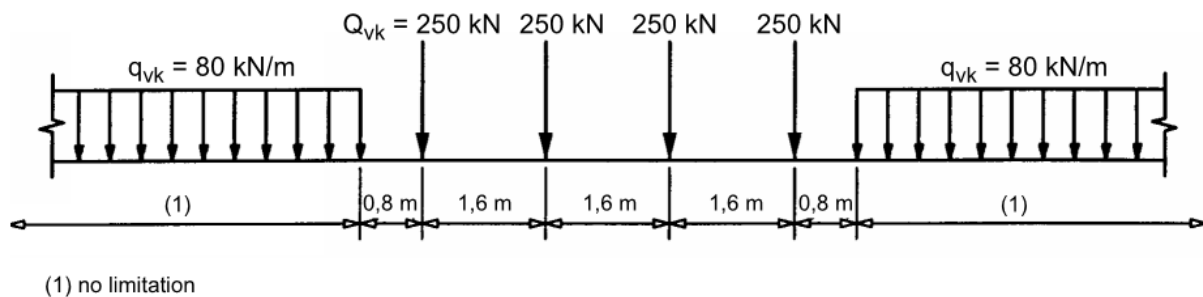


Figure 1.3. UIC Load Model 71 (UIC71) (International Union of Railways 2006)

The Chinese specification uses the Chinese ZK load (which is 80% of the UIC71 load) for typical high-speed rail bridges (Figure 1.4).

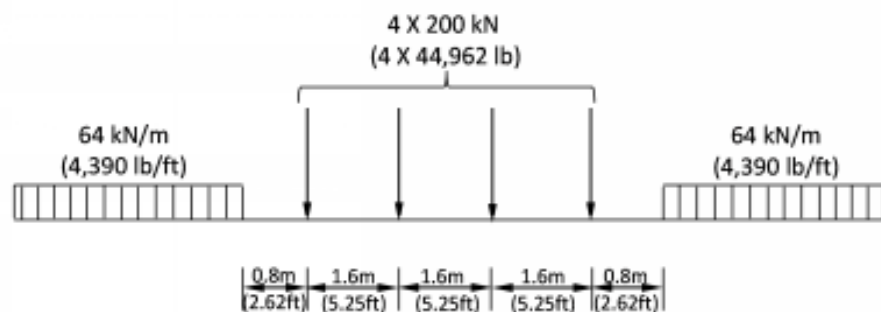


Figure 1.4. Chinese ZK load (Zhou et al. 2012)



1.1.3. SERVICEABILITY LIMITS

The serviceability limit states for high-speed rail address the same response quantities as do the limits specified in conventional rail codes, but the limiting values are more stringent due to the higher train speeds. Serviceability limits from the California, Chinese, and European design standards will be compared in this section.

1.1.3.1. VERTICAL DEFLECTION LIMITS

Many countries limit static vertical deflections of bridge decks as an indirect way to mitigate undesired vehicle acceleration. The deflections are computed assuming static behavior in the interests of simplicity, with an amplification factor to account approximately for the dynamic behavior. The vertical serviceability load cases and limits differ from country to country. For example, Eurocode suggests a limit based on a single loaded track considering a dynamic impact factor; meanwhile, the Chinese code provides limits based on two tracks loaded but does not consider dynamic impact. In general, deflection limits are a function of train speed, span length, type of track (ballasted or ballastless), and span type (simply supported or continuous). A summary of requirements from a few design standards is provided in Table 1.3. All limits reported in the table are for the highest design speeds designated.

Table 1.3. Load cases and limits for static vertical deflection

Design Standard	Load Case	Δ/L limit (ranges based on span)
Eurocode/UIC	Single track loaded UIC Load Model 71 with dynamic impact factor	1/2650-1/1500 (3+ simply supported spans) For continuous beams, adjust the limit with factors
China	Two tracks loaded ZK design live load (80% of UIC71 load) on each track No dynamic impact considered	1/1600-1/1500 (3+ simply supported spans) For continuous beams or single-track bridges, adjust the limit with factors
CAHSR	Check both 1 and 2 tracks loaded (2-track case usually controls) Modified Cooper E-50 maintenance train load with dynamic impact	Single track: 1/3500-1/2200 Double track: 1/2400-1/1100 (All types of spans)

A visual comparison of the different deflection limits vs. span length is shown in Figure 1.5. Note that here, they are expressed as span/deflection so that the linear features of the equations are apparent. The CAHSR deflection limit is stricter than the Eurocode/UIC limit for all span lengths. The CAHSR deflection limit is also stricter than the Chinese limit for spans under 200 ft, which are the most common span lengths used.

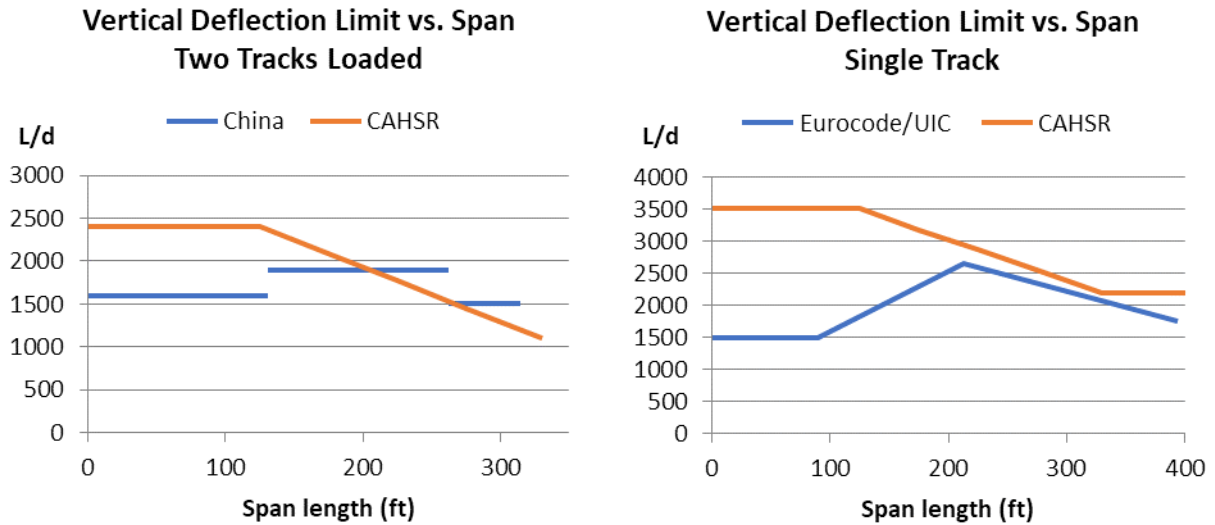


Figure 1.5. Comparison of vertical deflection limits vs. span length

1.1.3.2. ROTATION LIMITS

While the design standards limit vertical deflections to minimize passenger discomfort, they also specify rotation limits to keep the rail operational. End rotations impose additional axial and bending stresses on the rail, which can damage the rail fasteners. The rotations may also cause abrupt angular changes in track geometry, which leads to passenger discomfort (in mild scenarios) to train wheel unloading in more severe cases (California High-Speed Rail Authority 2019). These rotation limits are applied to the same load cases as the deflection limits. The Chinese code limits rotation at the beam end depending on track type, location of beam end, and beam end overhang length (see Figure 1.6 and Table 1.4). The units are expressed in milli-radians, and L_e is the beam end overhang length.



Figure 1.6. Sketch showing the rotation angle to be limited (He et al. 2017)

Table 1.4. Rotation limiting values for Chinese HSR bridges, where L_e is the beam end overhang length.

Track type	Location	Limiting value (rad)
Ballasted	At abutment	$\theta \leq 2.0 \text{ } \text{‰}$
	At pier	$\theta_1 + \theta_2 \leq 4.0 \text{ } \text{‰}$
Ballastless	At abutment	$\begin{cases} \theta \leq 1.5 \text{ } \text{‰}, & L_e \leq 0.55 \text{ m} \\ \theta \leq 1.0 \text{ } \text{‰}, & 0.55 \text{ m} \leq L_e \leq 0.75 \text{ m} \end{cases}$
	At pier	$\begin{cases} \theta \leq 1.5 \text{ } \text{‰}, & L_e \leq 0.55 \text{ m} \\ \theta \leq 1.0 \text{ } \text{‰}, & 0.55 \text{ m} \leq L_e \leq 0.75 \text{ m} \end{cases}$

The CAHSR code has similar rotation limits, which are outlined in Table 1.5. There is no distinction between track type or location.



Table 1.5. Rotation limiting values from CAHSR Design Criteria

Load Case	θ (rad)
1 track loaded	1.2 ‰
2 tracks loaded	1.7 ‰

Typically, the rotation limits will only control superstructure selection for longer spans. Otherwise, vertical deflection and acceleration will likely control. Additional details on the controlling limits are provided in Section 1.1.4.4.

1.1.3.3. VERTICAL ACCELERATION LIMITS

The acceleration limit is one of the common criteria that controls bridge design. It exists to ensure track alignment, track stability, and passenger comfort (Andersson and Karoumi 2015). The modeling of the dynamic effects of the train, bridge, and possible ballast to analyze deck acceleration can be complex and varies depending on the design standard, and it will not be discussed here. Analysis results are then compared with the general acceleration limits summarized in Table 1.6.

Table 1.6. Load cases and limits for vertical acceleration

Design Standard	Load Case	Acceleration Limit
Eurocode/UIC	Single track loaded UIC High Speed Load Model (HSLM) or actual service train	Ballasted: 0.35 g Non-ballasted: 0.5 g
China	Single track loaded Actual service train	Ballasted: 0.35 g Non-ballasted: 0.5 g
CAHSR	Single track loaded Actual service train	0.5 g

1.1.3.4. VERTICAL NATURAL FREQUENCY BOUNDS

Natural frequency also needs to be limited to avoid resonance between the bridge and vehicle. UIC, China, and CAHSR all provide limits on the first natural frequency of vertical deflection. If girders do not satisfy the bounds, then additional train-structure dynamic analysis is required. The natural frequency limits for UIC and CAHSR are the same, which include an upper and lower bound. The lower limit is:

$$n_0 = \begin{cases} \frac{80}{L}, L \leq 20 \text{ m} \\ 23.58L^{-0.592}, 20 < L \leq 96 \text{ m} \end{cases}$$

And the upper limit is:

$$n_0 = 94.76L^{-0.748}$$

where the frequency, n_0 , is in Hz and the span, L , is in meters.



These specifications were developed for UIC primarily for train speeds below 250 km/h (155 mph), but then applied to HSR as well (Zhou et al. 2012). Chinese engineers deemed the UIC lower bound not strict enough to prevent excessive vibration or resonance due to high-speed trains. Chinese studies also concluded that an upper limit is not necessary since tight construction tolerances would mitigate potential issues due to higher fundamental frequencies (Zhou et al. 2012). The Chinese lower frequency limits for common spans are listed in Table 1.7. As can be seen, higher vehicle speeds require more stringent frequency limits. Longer spans have inherently lower natural frequencies, and the lower frequency limits associated with them reflect this fact.

Table 1.7. Chinese lower bound frequency limits for common spans

Span Length, m (ft)	Design Speed, km/h (mph)		
	250 (155)	300 (186)	350 (217)
12 (39)	100/L	100/L	120/L
16 (52)	100/L	100/L	120/L
20 (66)	100/L	100/L	120/L
24 (79)	100/L	120/L	140/L
32 (105)	120/L	130/L	150/L

A graphical comparison of the UIC and Chinese natural frequency limits is shown in Figure 1.7. The actual natural frequency of an example simply supported prestressed concrete HSR bridge is plotted alongside these limits. This natural frequency was calculated using the following equation:

$$n_0 = \frac{\pi}{2L^2} \sqrt{\frac{Er^2}{\rho}}$$

Where:

n_0 = natural frequency

L = span

r = radius of gyration

E = modulus of elasticity

ρ = mass density

This can also be expressed as:

$$n_0 = \left(\frac{\pi r}{2h} \sqrt{\frac{E}{\rho}} \right) \left(\frac{1}{L} \right) \left(\frac{h}{L} \right)$$

Where h = cross-section depth.



This arrangement of terms isolates key parameters into three groups. Assuming common material properties for a simply supported prestressed concrete HSR girder, the first group remains nearly constant. If the natural frequency limits are limited to a multiple of $(1/L)$, as done in the Chinese code, then the second group is constant as well. Therefore, the maximum L/h ratio is fixed, and hence, the example bridge and China lower natural frequency limits follow the same curve in Figure 1.7.

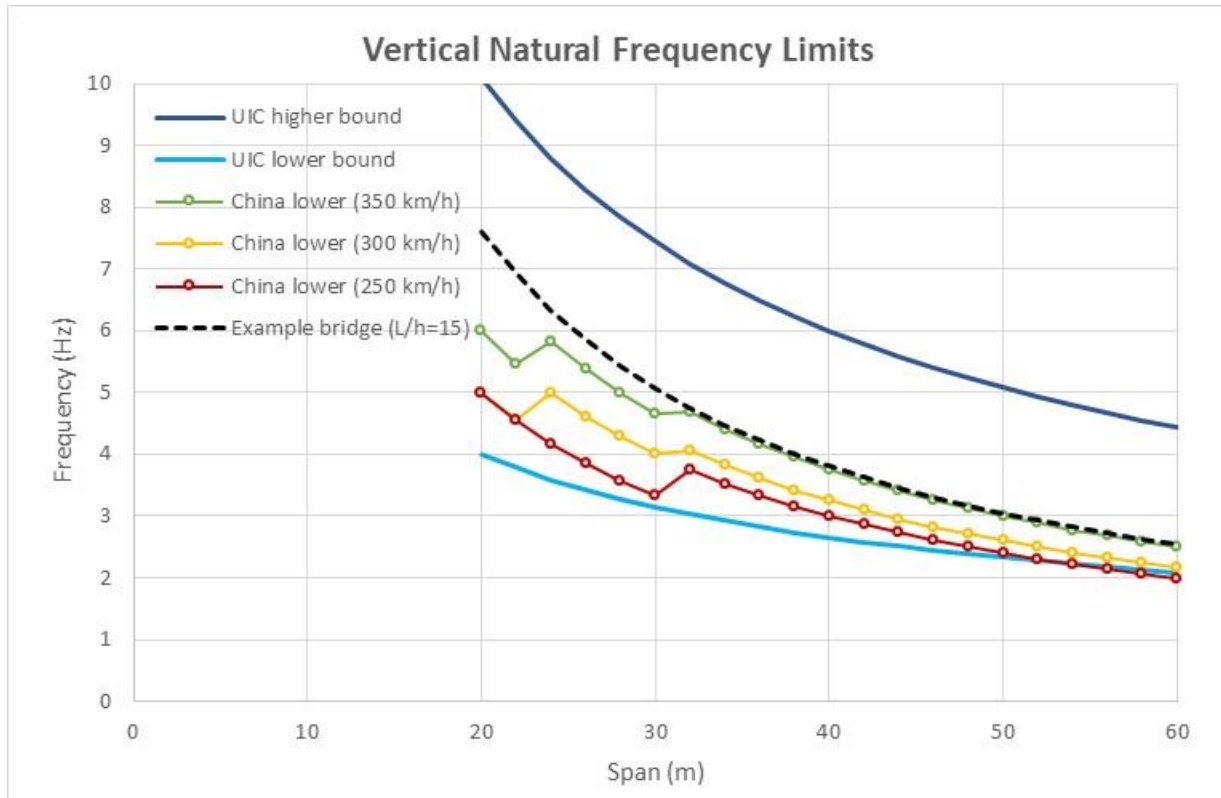


Figure 1.7. Comparison of vertical natural frequency limits from UIC and Chinese code. The “example bridge” curve shows the natural frequency of a simply supported HSR bridge with typical cross-section and material properties.

1.1.4. SUPERSTRUCTURE SELECTION

The strict serviceability criteria discussed in the previous sections imply the need for a stiff superstructure. Commonly, this need is addressed with a deep prestressed concrete box girder. While this cross-section helps satisfy serviceability criteria, it is much heavier than typical highway bridge sections and thus leads to issues with construction and seismic performance. The superstructure selection process to arrive at this typical prestressed concrete box girder as well as resolutions to construction and seismic issues, will be discussed in this section.



Lateral displacement and rotation limits also exist but are not discussed here. Among the serviceability limit states, the vertical deflection and acceleration limits most commonly control superstructure selection for short- to mid-length bridges. The influence of these limits on preliminary design will be discussed.

1.1.4.1. MATERIALS

Concrete is much more common than steel for all HSR bridges around the world. Concrete HSR bridges are generally cheaper and require less frequent maintenance than steel bridges. Construction procedures for concrete HSR bridges are well-known, and engineering knowledge has been thoroughly developed (Manterola and Escamilla 2014).

On the other hand, steel can be preferable for long spans or where low girder height and light structural weight are needed. Steel may also be beneficial on sites with tough terrain for construction purposes, where prefabrication of members eliminates the need for formwork or shoring (Minami and Shimizu 2011). However, the lighter weight of steel structures leads to higher levels of vibration, which can cause fatigue damage.

Composite steel and concrete superstructures are also possible and can provide the necessary stiffness while reducing structural mass. They are used in areas with poor soil quality and in seismic areas. Existing composite HSR superstructures include steel box girders with a concrete deck (Zhou et al. 2012), composite trough made of steel webs and a concrete lower chord (Kang et al. 2018) as shown in Figure 1.8, or steel box girders with concrete on both the top and bottom flanges.



Figure 1.8. The Ingolstadt Rail Bridge, which is a composite trough bridge (Image credit: Janberg (2020))

1.1.4.2. SPAN ARTICULATION

The most common type of HSR superstructure is a simply supported beam. However, continuous beams have also become increasingly used in recent years. Continuous spans are stiffer than simply-supported spans of equal proportions, meeting both static and dynamic criteria more efficiently (Kang et al. 2018). At the same time, they are more complicated for developing post-tensioning between spans and for analyzing secondary moment effects. Longer spans also require rail expansion devices, which impact rider comfort and require additional maintenance. For these reasons, some countries prefer shorter simply-supported spans as opposed to longer and fewer



continuous spans (Combault 2013). Meanwhile, Germany is shifting away from simply-supported bridges and towards continuous beams (Kang et al. 2018).

Continuity can also be provided between the spans and the columns. This results in a moment connection at the span-column joints, taking advantage of frame action and thus reducing demands on the foundations. Since the superstructure and columns are monolithic, there are no bearings, eliminating the risk of unseated spans during seismic events and the need for bearing maintenance. On the other hand, this fixity introduces moments caused by creep, shrinkage, and thermal effects. The construction of the superstructure-column joints is also more complicated with a fixed connection. This type of continuity has been used on some bridges in the Taiwan High Speed Rail system (Parsons Brinckerhoff 2009).

1.1.4.3. CROSS-SECTIONAL SHAPE

The most common cross-sectional shape for HSR bridges is a box girder, which efficiently provides the bending and torsional stiffness required to satisfy serviceability criteria. Both single- and double-cell box girders have been used, with the single-cell facilitating maintenance inspection more easily. Other common cross-sectional shapes and their benefits and drawbacks are outlined in Table 1.8. As an alternative to existing HSR superstructure configurations, a series of I-girders with a small top flange and large bottom flange may also be considered (Figure 1.9). This is similar to the I-girder in Table 1.8, but has optimized the relative flange sizes for flexural stiffness. By doing so, a smaller section can be used to provide the same stiffness as a larger typical I-girder. As a result, the girders can be precast in a plant and transported to site without special accommodations. This section shape would need to be further refined before it is implemented but is a promising option for accelerated bridge construction of HSR structures.

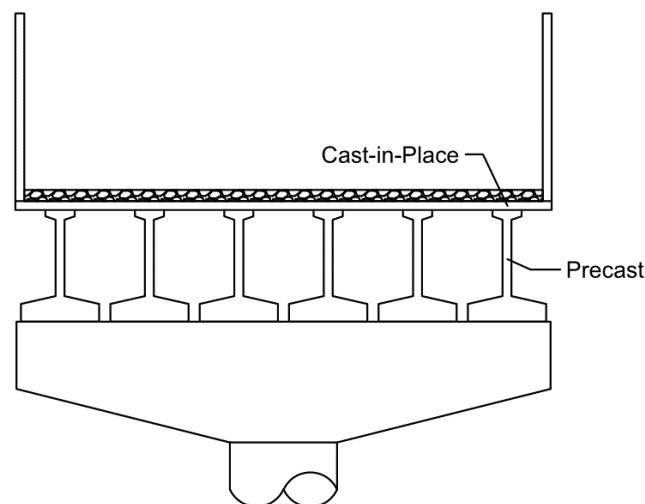


Figure 1.9. Alternative HSR cross-section



Table 1.8. Comparison of girder shapes (Evangelista and Vedova 2009)

Shape	Drawing	Pros	Cons
Box girder		<ul style="list-style-type: none"> -High flexural and torsional efficiency -Often less pre-stressing costs 	<ul style="list-style-type: none"> -May be visually unappealing
U-girder or tub girder		<ul style="list-style-type: none"> -Built-in noise reduction and train containment -Track level is at a lower elevation, meaning that embankments can be smaller -Lower track profile also shortens the moment arm for horizontal loads, resulting in smaller moments in the substructure 	<ul style="list-style-type: none"> -May require more concrete (and thus self-weight) than the box girder since it is less efficient
I-girders		<ul style="list-style-type: none"> -Feasible to precast girders off-site -Precasting may allow for faster production -Lighter loads for setting girders (may be beneficial where crane access is limited) 	<ul style="list-style-type: none"> -Need separate deck placement and connection after girders are set

1.1.4.4. SPAN-DEPTH RATIO

A study was performed to examine the typical span-depth ratio required in order to satisfy the CAHSR static serviceability criteria. A typical HSR prestressed concrete box girder section was assumed as a starting point. Then, the web height of the section was increased until static deflection and rotation criteria were satisfied for a given span. Natural frequency limits are also checked. This simple procedure was repeated for multiple span lengths and for simply supported, fixed-fixed, and 3+ continuous spans. The CAHSR criteria do not distinguish between support conditions, so the criteria remained the same across the different boundary cases. The results of the study are summarized in Figure 1.10, which shows the results derived from static deflection and rotation criteria.

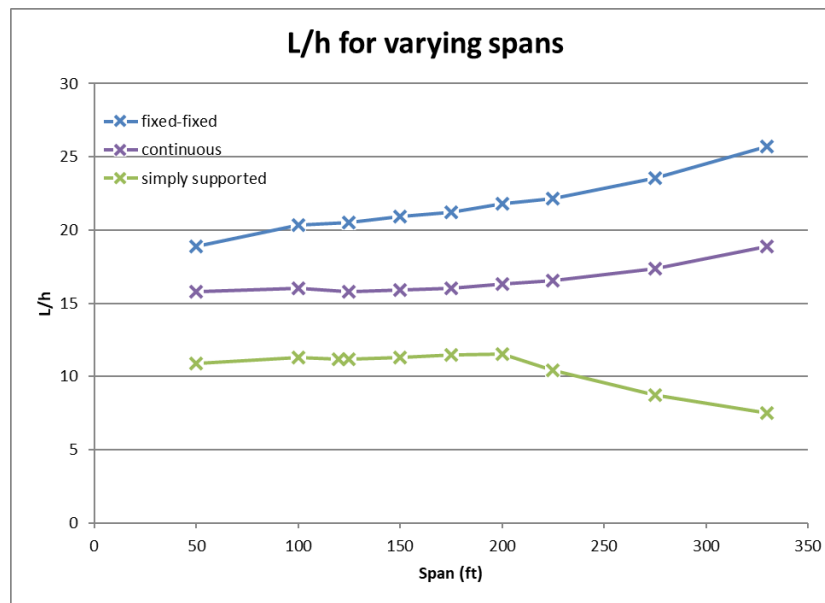


Figure 1.10. Required span-depth ratios based on CAHSR Design Criteria

The CAHSR limits lead to girders with a low span-depth ratio relative to that of highway bridges (e.g., $L/h \approx 10$ for short simply supported spans). For spans under 200 ft., the deflection limit was the controlling criterion; for spans greater than 200 ft., end rotation controlled. Natural frequency limits did not control for any simply supported spans, although they led to L/h ratios that were quite close to those dependent on deflection. For the fixed-fixed and continuous spans, all configurations had fundamental frequencies that exceeded the upper limit; this indicates that further analysis is needed to determine whether the fundamental frequency is acceptable or not. The precise reason for the upper limit is also unclear. The only explanation found was “the upper bound is to limit train-track dynamic responses due to track irregularities” (Zhou et al. 2012).

While this study was performed using a generic box girder section and CAHSR limits, most existing HSR concrete girder bridges have span-depth ratios similar to those in Figure 1.10. This demonstrates that the stringent track serviceability criteria are a significant driver for the cross-sectional depth of HSR bridges.

1.1.4.5. CONSTRUCTION METHODS

Construction methods can also influence the superstructure selection process, and vice versa. Many HSR bridges are cast-in-place (CIP), though segmental precasting and full-span precasting have been implemented as well. Existing HSR bridge construction methods are similar to highway bridge construction methods but occur on a larger scale. They include full staging with falsework, using a movable scaffolding system (MSS), cantilever construction, incremental launching, and rotation construction (Dong Kang and Suh 2003; Sobrino 2008; Yan et al. 2015)



Precasting of HSR bridges can lead to significant time savings, better quality control, and possible cost savings depending on the scope of work. In spite of the bulky superstructures, full span pre-casting of HSR bridges has been utilized in Italy, Taiwan, and Korea. Most commonly, precast facilities are located near the bridge site(s) and are specifically designated for HSR bridge construction. The spans are handled using custom equipment. For example, portal cranes are used to move the spans around the precast facility; special tire trolleys then transport the spans to site; and finally, a self-launching gantry positions and erects the span (Rosignoli 2016; Tai et al. 2010). In Taiwan, spans can also be transported from the storage yard to site either directly with portal cranes (bypassing the need for a transport trolley), or with a transportation trolley that has built-in hoisting equipment (so no portal crane is required). An example of a transportation trolley with lifting capability is shown in Figure 1.11.



Figure 1.11. Transporter with hoisting equipment used in Taiwan (Tai et al. 2010)

Due to the specialized equipment and potential need for new casting facilities, the up-front costs for precast are generally higher than for CIP structures. However, the time and material savings (due to less material wastage and tighter quality control) are significant and can offset the initial costs for larger scopes of work. In Korea, contractors estimate that on a bridge over 3 km (1.96 mi) long, cost savings of 20-30% can be achieved (Dong Kang and Suh 2003). Therefore, precasting should be considered for longer HSR bridges or where an expedited schedule is necessary.

1.1.4.6. CONCLUDING REMARKS

The superstructure selection process was outlined in this section. Material selection, span articulation, cross-sectional shape including span-depth ratio, and construction methods were discussed. Existing bridges demonstrate that a wide variety of superstructure types and construction methods can be used for HSR bridges; however, the most commonly used superstructure and construction method is a simply supported, CIP, post-tensioned concrete box girder.



1.2. SUBSTRUCTURE SYSTEMS

The substructure systems including piles, shafts, columns and column tops, pile tops are often built using Cast-In-Place concrete methods. The foundations that support the bridge columns can be classified into shallow and deep foundations. Considering a range of soil and rock properties can be encountered along the HSR lines to be constructed, different foundation types need to be considered to meet the strength/stability requirements and the cost effectiveness. In case the in-situ soil and rock conditions are competent, shallow foundations such as spread footings or mat foundations can be adopted, otherwise deep foundations such as drilled shafts and driven piles need to be considered. In areas of increasingly minimal soils, either Cast-In Drilled-Hole (CIDH) or Cast-In-Steel-Shell (CISS) piles can be used stretching down into capable material. The under reamed columns with various cross sections may be created using, e.g., bellings tool with retractable wings.

The foundation design should meet all necessary performance requirements as defined in AASHTO LRFD Bridge Design Specifications such as lateral earth pressure, excessive deformation, stability issue, uplift pressure for all limit states given the field condition. The scour potential also need to be considered wherever applicable, e.g., near the water crossings. The type of foundation and the impact of foundation installation on existing facilities and neighboring foundations also needs to be taken into account (Gingery et al. 2011). The load and resistance factor design (LRFD) based on the probability of failure or reliability is currently adopted in the California HSR construction project. In LRFD, the likelihood of a load exceeding the capacity of the foundation is considered during the entire life span, and the method considers the following three limit states for foundation design:

- *Serviceability Limit State* – Evaluation of performance that adversely affect the stability and displacement of the structure under normal service loads.
- *Strength Limit State* – Evaluation of limit states associated with the strength under various loading conditions.
- *Extreme Event Limit State* – Evaluation of strength and stability under extreme loading conditions caused by extreme events such as earthquakes.

1.2.1. FOUNDATIONS

1.2.1.1. SHALLOW FOUNDATION

While the shallow foundation such as spread footings or mat foundation may not be the primary choice for the bridge foundation, it can be adopted in case in-situ soil or rock properties are competent at a shallow depth or those competent properties can be obtained at a shallow depth after ground improvement. However, shallow foundations are not ideal for soils that are potentially unstable, e.g., expansive, liquefiable, etc. The Federal Highway Administration (FHWA) developed a Geotechnical Engineering Circulars (GEC) for analysis and design procedures for highway bridges supported on the shallow foundation (Kimmerling 2002). AASHTO LRFD Bridge Design Specifications (BDS) can be also referenced as the guidance with regional amendments based on the geotechnical properties obtained with field investigations.



1.2.1.2. DEEP FOUNDATION

Driven piles and drilled shafts are the two most widely used deep foundation types. California High-Speed Rail Authority Construction Packages discuss the requirements for some deep foundation types including micropiles as well as drilled shaft and driven pile. (See Book III, Part A. 1 - Design Criteria Manual by California High-speed Rail Authority (2015)). The design of deep foundations should be based on the project-specific data in the geotechnical reports obtained with the field investigations, and no presumptive values shouldn't be used such as International building code (IBC) presumptive allowable bearing pressures that defines the allowable bearing stresses depending on soil/rock classification (International Code Council 2015). The decision of deep foundation can be made per many factors. For example, if there are existing obstacles to perform pile driving, e.g., thick boulder layer, low headroom due to existing bridges and facilities, noise/vibration sensitive environment, drilled shafts may be more feasible. Also, if a single shaft can be used per column, it can be more economical than using a pile group with a pile cap. On the other hand, pile driving can be cost effective if some number of drilled shafts need to be installed per column. For example, in Taiwan, drilled shafts, also called as bored piles in the country, have been preferred to driven piles due to concern of vibration and noise to nearby buildings and facilities, considering Taiwan is one of the most densely populated country. With the reverse circulation method introduced in 1960s, the drilled shaft construction became a popular deep foundation. The reverse circulation drilling uses a dual wall drill where the inner tube is used to continuously discharge the drilled cuttings into the external collector system, and therefore provides a high penetration rate. With the full-length casing method introduced in 1990s in Taiwan, the drilled shaft installation became more efficient in case gravelly soil and bed layers exist, and therefore, around 30,000 piles were installed along the 345 km of Taiwan High Speed Rail (THSR) lines (Chin and Chen 2007). Table 1.9 shows the factor of safety adopted in the THSR foundation design. A large span bridge imposes a higher load on each column and in turn the foundation, for which a higher capacity deep foundation may need to be considered, e.g., barrette, caisson, etc. The barrette foundation is different in the sense that a diaphragm wall machine is used for installation and various cross sections can be constructed, e.g., rectangle, cruciform, H-shape, etc.

Table 1.9. Factor of safety used in the THSR foundation design (Chin and Chen 2007)

	Safety Factor		
	Normal Load	Exceptional Load	Ultimate Load
End Bearing Capacity	3.0	2.0	1.25
Skin Friction	2.0	1.5	1.25
Pullout Resistance	No tension forces are permitted on piles.	2.5	1.5

General rules for the construction shall be adhered to to achieve the high quality of the constructed foundations. For example, the bottom cleanliness of drilled shaft should be checked such that a minimum of 50% of the bottom of the shaft should have less than 0.5" of sediment at the



time of concrete placement, and a maximum depth of sediments at any place of the bottom should not exceed 1.5". The thickness of steel casing should have at least $\frac{3}{4}$ " in case permanent steel casing method is used for the drilled shaft construction. In with the geotechnical report, the groundwater properties should be included so that corrosion susceptibility can be determined ahead. If the shafts are to be placed in an aggressively corrosive environments, support from the steel casing should not be expected in a long-term. At least 6" offset should be considered at the top of the shaft if the drilled shaft has a diameter larger than 5'. Further details can be found in *Standard Specification on Drilled Concrete Piers and Shafts*. The micropiles can be designed per AASHTO LRFD BDS with California Amendments, Article 10.9: Micropiles and FHWA-SA-97-070 (Tom Armour et al. 2000).

1.2.1.3. MICROPILE FOUNDATION

Micropile has been used for foundation retrofit. A literature shows on a micropile-based foundation seismic retrofit of the Boeing field control tower in Seattle, Washington (Parmantier et al. 2004). The original construction built in the 1960s was founded on timber piles of unknown length and soil borings performed indicated liquefiable soils in the depths of approximately 35 feet. The foundation retrofit included the use of drilled shafts adjacent to the tower, which was tied to new structural steel bracing which was added to increase the tower to overturning during design earthquake loading. The drilled shafts were placed outside the existing pile cap and consisted of dimensions 4 in diameter and 45 ft in depth. The pile configuration involved placing groups of four drilled shafts on the east and west side of the foundation.

Another case study demonstrated the use of micropile-based foundation groups in San Francisco bay area (Momenzadeh et al. 2013). The foundation retrofit consisted of the use Type "D" micropile groups through an existing foundation pile cap at 5 existing bents. The micropiles were one foot in diameter and consisted of high yield 2.25" treated steel rod extending over the entire length of the pile and a 9 5/8" diameter high yield N80 steel casing extending down to approximately the top of the bonded length of the pile. The micropiles were then subsequently load tested to confirm design assumptions. The piles performed well and reached close to the design limit of 0.5 inch in compression. Load testing also confirmed that under cyclic loading, the displacement shall not exceed the tension dead load, or the risk of pile failure is imminent.

There are two different design mechanisms contributed by micropiles when used as foundation supporting elements, which are (a) Direct structural support (Case 1 micropiles) and (b) Soil reinforcement (Case 2 micropiles). Case 1 micropiles are commonly referred to the case where vertically installed micropiles are directly supporting the foundation load. On the other hand, Case 2 micropiles are typically a network of reticulated elements working as a composite pile-soil foundation by encompassing and reinforcing the internal soil (Shu and Muhunthan 2010). On the other hand, (c) a third type of mechanism (hereafter, referred as Case 3) may be developed to 'significantly' enhance overall seismic performance of bridge in high seismic areas: The mechanism is realized by utilizing the dampers installed between the existing foundation and neighboring 'micropile islands'. This design was inspired by the micropile foundations with prefabricated caps used for transmission towers against high winds (American Galvanizers Association 2012). As the



prefabricated cap is used along with the rapid micropile installation, the construction is fast. Furthermore, the seismic retrofit can be easier for the bridge foundations in locations with limited access. Use of micropiles in seismic areas has many advantages as the system provides great ductility and flexibility. Case 3 mechanism may be combined with the other types of design mechanism (i.e., Case 1 or 2) to increase the resistance against the increased load due to HSR. Researchers have reported that use of micropiles have many benefits for bridge constructions (Herbst 1994; Mason 1993; Pearlman et al. 1993). Figure 1.12 shows an example of using micropiles to enhance the performance of bridge foundation, in which a group of 4 micropiles with a diameter of 0.25 meters was used to enhance the foundation of 6 piles. Alfach (2019) showed the overall improved foundation performance with the battered pile fixed to the cap.

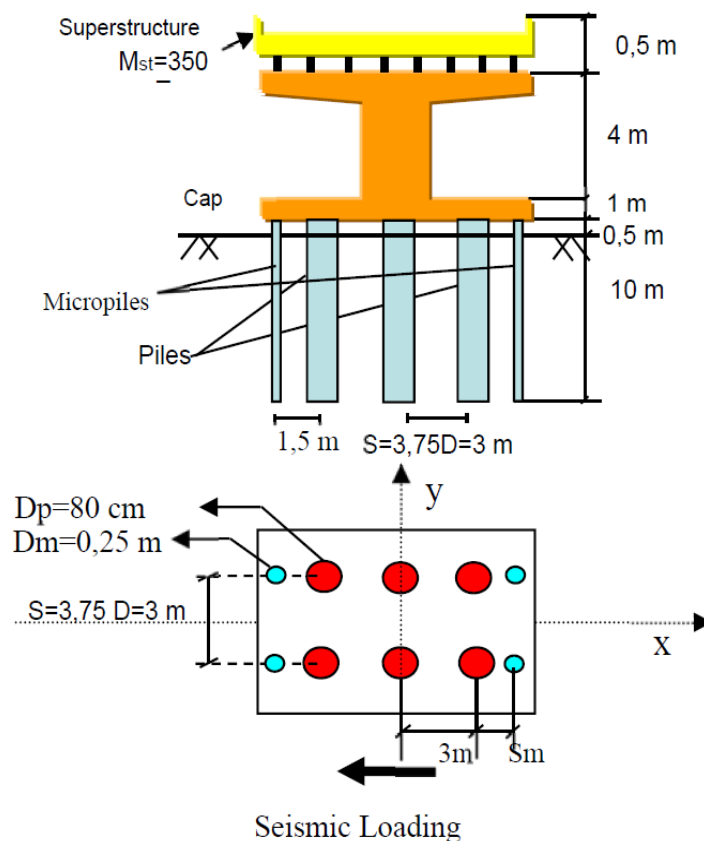


Figure 1.12. Bridge foundation reinforcement using micropiles (Alfach 2019)

1.2.2. DRAINAGE

Bridge drainage path can be designed by sloping the deck and the girders in the superstructure, from which the water is gathered and passed on to a funnel cast into the concrete substructure, and then pier columns and abutment walls to the foundations. However, it is important that the drain pipes do not go through the potential plastic hinge areas. Further details can be found in the Drainage chapter in California High-Speed Rail Authority Construction Package 4.



1.2.3. GEOTECHNICAL DEMAND

1.2.3.1. UPLIFT AND DOWNDRAG FORCES

No net uplift force shall be acceptable for shallow foundations under any load combinations. On the other hand, no net uplift force is expected for deep foundation piles and multi-column bents under service load combinations, while the net uplift is allowable for ultimate limit states and extreme load conditions. In case the Maximum Considered Earthquake (MCE) counteracts 50% of the dead load action, hold-down gadgets should be implemented to lower it to less than 10%, where the dead load refers to the dead load of structural and non-structural components as well as the permanent attachments. Potential downdrag on the deep foundations also should be taken into account. The CA HSR authority requires to document the required negative skin friction in the geotechnical report. Further details can be found in the Geotechnical chapter in California High-Speed Rail Authority Construction Package 4 (California High-speed Rail Authority 2015) or AASHTO LRFD BDS with California Amendments Article 3.11.8.

1.2.3.2. GROUND MOTIONS

Both Maximum Considered Earthquake (MCE) and Operating Basis Earthquake (OBE) should be considered in the design against seismic excitations. Per CA HSR Construction Package 4, MCE is defined as “ground motions corresponding to greater of (1) a probabilistic spectrum based upon a 10% probability of exceedance in 100 years (i.e., a return period of 950 years); and (2) a deterministic spectrum based upon the largest median response resulting from the maximum rupture (corresponding to M_{max}) of any fault in the vicinity of the structure” and OBE is defined as “Ground motions corresponding to a probabilistic spectrum based upon an 86% probability of exceedance in 100 years (i.e., a return period of 50 years).” Figure 1.13 shows a design spectra for elevated structures adopted in CP4.

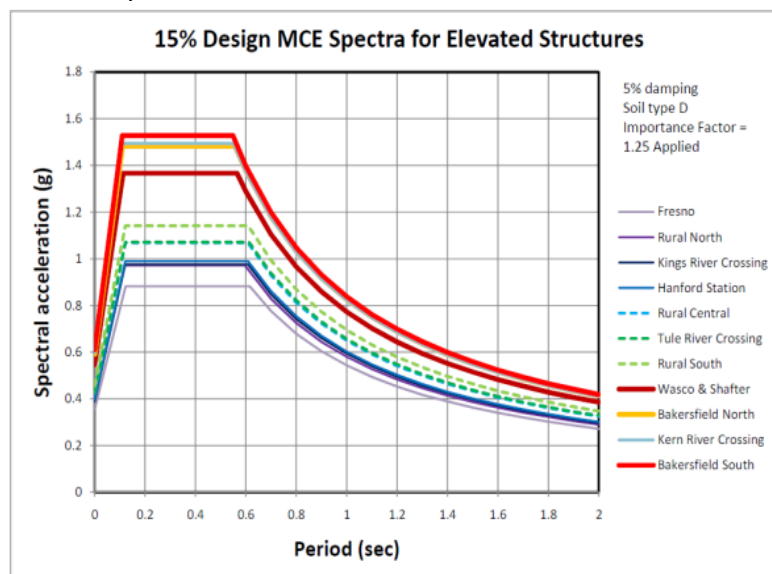


Figure 1.13. Design Spectrum of CP4 (California High-speed Rail Authority 2015)



1.2.3.3. EARTH PRESSURES

Vertical and lateral earth pressures along with other soil parameters should be determined to design the substructure elements. Loading from neighboring buildings or facilities shall be also considered for the estimation. The maximum depth should be considered to estimate the vertical earth pressure including ground surface, roadway crown, etc. To be on the conservative side, 100% of saturation ratio should be considered when estimating the soil unit weight.

The lateral static earth pressure shall be typically calculated for cantilever retaining walls which have the base and a free end that is not restrained against any lateral pressure. This deformation of the free end should not exceed $0.004H$ where the height 'H' is defined as the wall height from the base to the top. The limit states need to be computed based on the active and passive failures. While the aforementioned type of retaining wall is called as a yielding wall, the rigid wall is a type restricted at the top to control the deflection associated with the active pressure failure. The permanent lateral earth pressure for the walls can be estimated assuming equal fluid pressures at-rest and the Mohr-Coulomb yield criterion.

1.2.3.4. GROUND SETTLEMENT

Ground settlement includes elastic and plastic settlement including soil consolidation is caused by sustained loading and/or the temporal train-track interactions. The settlement is measured from the top of foundation, and the tolerable settlements need to meet the requirements in accordance with AASHTO LRFD Bridge Design Specifications. While there is no specific settlement requirement for MCE events, settlement limits under OBE loads are specified as shown in Table 1.10 where the allowable settlement for foundations is limited such that it should not exceed the sum of estimated settlements under the service 1 and OBE loads which includes post-liquefaction down drag, etc. The maximum horizontal drift between the top and bottom of a deep foundation is typically limited to less than 1.75" under OBE loading (Gingery et al. 2011). Further discussions on the settlement requirement may be found Section 12.8.6.18 in the Geotechnical chapter in CA HSR Authority Construction Package 4 (California High-speed Rail Authority 2015).

Table 1.10. Settlement limits for the combined service 1 and OBE loads (Gingery et al. 2011)

Settlement Criteria	Non-Ballasted Track	Ballasted Track
Differential settlement between adjacent supports ¹	$\leq L/1500$ and $3/4"$, where L = smaller span	N/A ³
Differential settlement between the abutment and approach embankment ²	$\leq 3/8"$ over 62 feet	$\leq 3/4"$ over 62 feet
Differential settlement between the abutment and tunnel portal	$\leq 3/8"$ over 62 feet	N/A ³
Uniform settlement at piers and abutments	$\leq 3/4"$	N/A ³

**Notes:**

1. The additional forces imposed on the structural system by differential settlements shall be calculated and considered as part of dead load in the design.
2. Prior to placement of tracks, the approach embankment shall be instrumented and monitored for a period of at least 6 to 12 months to ensure the embankment is in compliance with the settlement requirements set forth in the table above.
3. Not applicable based on the assumption that ballasted track will not be used for bridges, aerial structures or tunnels.
4. The settlements are calculated from the Service 1 load combination plus any settlements resulting from the OBE load combination (such as those resulting from post-liquefaction downdrag, seismic compaction, etc.).

1.2.3.5. HYDRAULIC PRESSURE

The impact of groundwater pore pressure caused by various hydrostatic and dynamic effects including buoyancy, wave loading and others should be considered in accordance with the requirements specified in Section 3.7 of the CBDS (Caltrans Bridge Design Specifications). To construct underground systems and the substructure of aerial systems and dwellings, including foundations and piling, The uplift pressure caused by the groundwater flow shall be considered with the highest water table location for conservative potential energy estimation or the extreme flooding condition described in the hydrologist report. The capacity of the structures against the uplift pressure can include the weight of constructed structures and other permanent dead loads. The possibility of design scour should be consulted with hydrology engineers and needs to be investigated in accordance with AASHTO LRFD BDS with California Amendments Article 3.7.5 (California High-speed Rail Authority 2015).



2. HSR BRIDGE NUMERICAL MODELING STRATEGIES

This section presents the process of formulating a sophisticated train-track-structure interaction model of a prototype HSR system. A prototype bridge, track, and train system were selected from the studies researched in the literature search. The prototype track-bridge system was selected based on the completeness of the design guideline provided in the reference study, such as bridge dimensions and cross-sectional properties. Assumptions were made where information was omitted in the reference study. This was not a major issue because the purpose of this study was to demonstrate how to model an HSR system as opposed to discuss or assessing the viability of a certain design. Similarly, the prototype train system was selected from a reference study that explicitly stated the masses of the various train components, as well as the stiffness and damping properties of the primary and secondary suspension systems, which are critical to accurately simulating the dynamic behavior of an HSR system.

2.1. SELECTION OF PROTOTYPE HSR SYSTEM

2.1.1. TRAIN SYSTEM PROTOTYPE

The prototype train system selected for this study is the KTX-Sancheon high-speed train which is shown in Figure 2.1. Formerly known as the KTX-II, the KTX-Sancheon is the second commercial high-speed train operated in South Korea as part of the Korea Train eXpress (KTX), making its debut in 2010. The KTX-Sancheon consists of two power cars at both ends and an articulated set of eight intermediate passenger cars in-between. As mentioned previously, an articulated bogie system couples a passenger car with the fore and rear passenger car, improving riding conditions of the train. As can be seen in Figure 2.1, the power cars have two standard bogies, and the extreme intermediate passenger cars have a standard bogie and an articulated bogie coupling them with the intermediate passenger cars.



Figure 2.1. Photo of KTX-Sancheon (Kim 2014).

2.1.2. TRACK AND BRIDGE SYSTEM PROTOTYPE

The prototype track-bridge system selected for this study is a ballastless track prestressed concrete double-track simply supported girder bridge used in a publication by Li et al. (2020). The track-bridge system is from the Beijing to Xuzhou section of the Beijing-Shanghai high-speed railway. The bridge has 10 equal spans of 31.95 m with a total length of 319.5 m. The bridge superstructure is made of C50 concrete and is 13.40 m wide at the top, 5.74 m wide at the bottom, and 3.09 m deep from the top to bottom surface. Each girder end is supported by two spherical steel bearings that rest on the 11 single column bents of 13.5 m height, made of C50 concrete and HRB335 steel bars. The bridge properties and overview as obtained from the reference study is shown in Figure 2.2.

The CRTS II slab ballastless track was adopted for the track system and comprises of base plates, track plates, rails and connecting members. The connecting members include sliding layers, shear cogging, CA layers, shear reinforcement, fasteners, and lateral blocks. The CHN60 rails are fixed to the base plate through WJ-8C fasteners. The track plate is made of C55 concrete and has a width and thickness of 2.55 m and 0.20 m, respectively. The track plate is connected to the C30 concrete base plate of 2.95 m width and 0.19 m thickness through the CA layer. Shear reinforcement bars are placed at the girder ends in the CA layer to withstand the deformation caused by rotation, and the sliding layer is arranged between the bridge deck and the base plate. The sliding layer, CA layer and fasteners allow for longitudinal slippage relative to the bridge and the lateral blocking provides support in the transverse direction relative to the bridge. The layout of the connection layers is shown in Figure 2.2(b) and Figure 2.3.

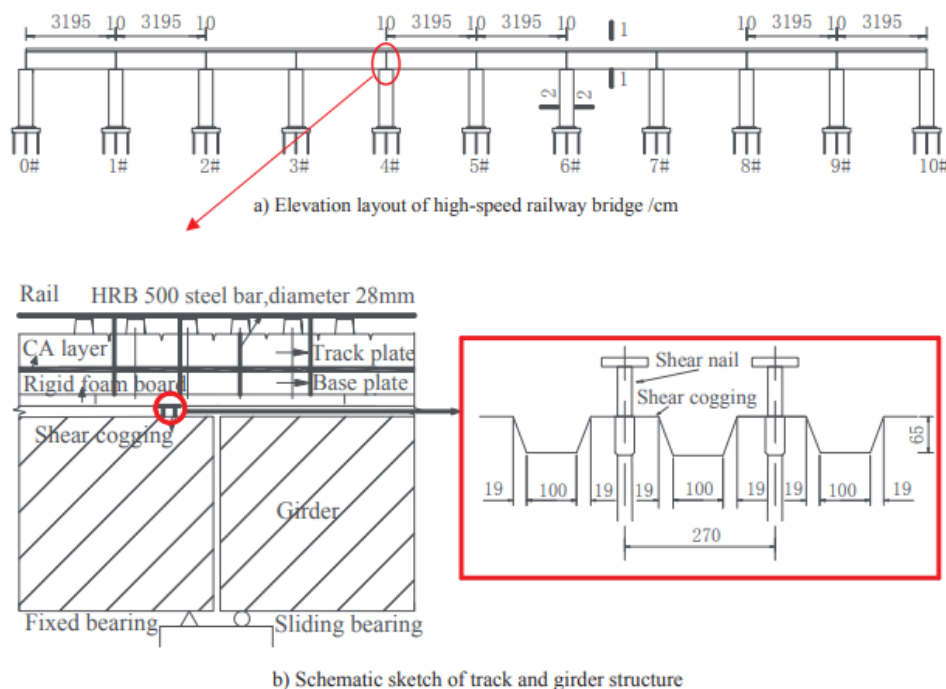


Figure 2.2. Schematic of the prototype bridge: a) Elevation layout of high-speed railway bridge/cm, b) Schematic sketch of track and girder structure (Li et al. 2020).

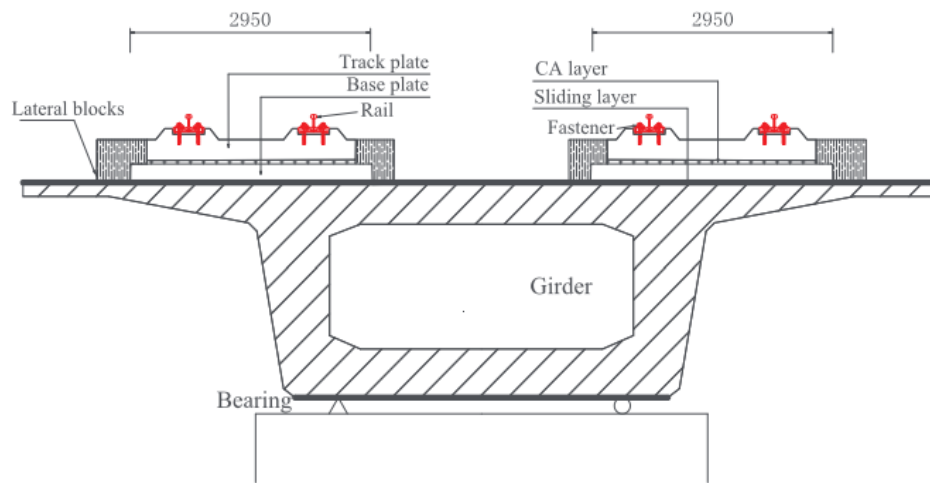


Figure 2.3. Schematic of typical bridge cross-section of track and girder structure (Li et al. 2020).

2.2. NUMERICAL MODEL IN OPENSEES

OpenSees is an object-oriented, open-source software framework that allows users to create both serial and parallel finite element computer applications for simulating the response of structural and geotechnical systems subjected to earthquakes and other hazards (Gregory L. Fenves et al. 2020). *OpenSees* allows the user to build a structural model by using the numerous commands available in the program. The commands used in the model for this study are discussed in this section.

2.2.1. BASIC MODEL DEFINITIONS

To start a model, the user must define the spatial dimensions (1, 2, or 3) and the number of DOFs (1, 3, or 6) at each node. Since a three-dimensional model was created for this study, the spatial dimension was specified as 3 and the DOF at each node was specified as 6 to account for all translational and rotational movement. The user can then construct numerous nodes which will be used to construct the framework of the structure. The node command requires a unique tag number and the x, y, and z-coordinates to define the location. *OpenSees* uses the numbers 1, 2, 3, 4, 5, and 6 to define the three translational and three rotational DOFs, respectively. For this specific model, the x-coordinates were modeled in direction 1, the y-coordinates in direction 2, and the z-coordinates in direction 3.

Single-point (SP) homogeneous boundary constraints can be implemented using the *fix* command, and multi-point (MP) constraint between nodes can be defined using the *equalDOF* command. The *fix* command is typically used at the base of the structure and was used at the foundation in this model. The *equalDOF* command was used to maintain structural stability between zero-length elements where stiffness was not defined for every DOF. The way in which the local coordinates of the elements correlate to the global coordinates of the model is defined using the *geomTransf* command. This command defines how *OpenSees* transforms the stiffness and resisting forces of the beam element from the local system to the global-coordinate system. Specifically, the basic linear geometric transformation method was selected for this study. Careful attention



should be given towards assigning the vector orientations for elements since this could result in element cross-section properties such as inertia in the local y and z axis to be flipped if defined incorrectly. A very helpful visual demonstration is provided in the OpenSeesWiki (Gregory L. Fenves et al. 2020) which should be referenced.

The next step is to define material properties used in the model. OpenSees has a wide variety of uniaxial materials, including steel and concrete materials. The `uniaxialMaterial` command is used to construct a material object which represents uniaxial stress-strain relationships (Gregory L. Fenves et al. 2020). `Steel01`, `Steel02`, `Concrete02`, `ViscousDamper` and `Elastic` material commands were used in this study to model the nonlinear behavior of the train, track, and bridge system components. The `Steel01` material was used to simulate the behavior of bearings and the connection layers in the track system. `Steel02`, `Concrete02` and `Elastic` materials were used to simulate the pier columns, and `ViscousDamper` materials were used to model the train suspension system. These materials were then specified as a parameter for the construction of elements.

Three types of elements were used in the model: elastic beam-column elements, displacement-based beam-column elements, zero-length elements, and two-node links. The elastic beam-column elements were used to model the elastic capacity protected elements like the bridge girder. This element command requires the section properties and not the material behavior because they remain elastic. Displacement-based beam-column elements were used to model the pier column. To accurately model the behavior of the columns, the cross-section must be modeled using the section fiber command. The patch and layer commands allow the construction of several fibers within a predefined cross-section to model the behavior of cover concrete, core concrete, and steel reinforcement with the material properties that were defined. The specific details will be explained later in Section 3.3.4.3. The fiber section can then be aggregated into an existing elastic material using the section aggregator command. The new aggregated material can then be used as the material parameter for the displacement-based beam-column elements. `zeroLength` element were used together with the `Steel01` material to simulate the bridge bearings and track connection layers. `twoNodeLink` elements were used together with the `ViscousDamper` material to simulate the damping in the train suspension system, and the stiffness in the train suspension system was simulated using an elastic material. A complete list of elements and materials used in the prototype model is presented in Table 2.1.

The mass of each component in the model can be defined using the mass command in OpenSees. The mass command allows the user to set the nodal mass values corresponding to each DOF. Defining masses allows the user to perform modal and dynamic analyses but is not required for static analysis. For this study, analysis of the modal and dynamic behavior of the structure was of interest, so the mass command was used to set translational and rotational mass values at every appropriate node. Mass values were applied at the nodes representing the centroid of the train system components and bridge footings, and the masses of the rest of the track-bridge system components were distributed at every node along the entire length of the rails, track and base plates, bridge girder, and pier columns.

Table 2.1. Prototype HSR Model Element and Material.



Components	Material	Element
Bridge		
Main Girder	Elastic	elasticBeamColumn
Footing	Rigid	elasticBeamColumn
Column-fiber Section	Concrete02	dispBeamColumn
	Steel02	
Foundation Springs	Elastic	zeroLength
Fixed Bearing	Steel 01	zeroLength
Sliding Bearing	Steel 01	zeroLength
Track		
Base Plate	Elastic	elasticBeamColumn
Track Plate	Elastic	elasticBeamColumn
Rail	Elastic	elasticBeamColumn
Sliding Layer	Steel 01	zeroLength
CA Mortar Layer	Steel 01	zeroLength
Fasteners	Steel 01	zeroLength
Shear Reinforcement	Steel 01	zeroLength
Lateral Blocking	Steel 01	zeroLength
Train		
Car Body	Rigid	elasticBeamColumn
Bogie	Rigid	elasticBeamColumn
Axle	Rigid	elasticBeamColumn
Axle Box Suspension	ViscousDamper	twoNodeLink
Secondary Suspension	ViscousDamper	twoNodeLink

2.2.2. TRAIN SYSTEM MODEL

To model the KTX-Sancheon, a study by Kwark et al. (2004) was used as a reference due to the similarity of the train prototype selected. The train selected by Kwark et al. (Kwark et al. 2004) is a Korean High-Speed Train (KHST) with an articulated bogie system. Based on the train configuration described in the study and the year the paper was published, the prototype train system selected by Kwark et al. (Kwark et al. 2004) was assumed to be the KTX-I, which is the first set of trains used by the Korea Train eXpress (KTX). The 20-car formation (380.15 m long) of the high-speed train entered service in 2004 and is optimized for high capacity. In comparison, the KTX-Sancheon is the second commercial high-speed train operated in South Korea and was created as a shorter companion to the KTX-I. Initially, the same train prototype was considered for this study; however, the train was exceptionally long (20 cars with a total length of 380.15 m) and was conceived as unfit for the prototype bridge selected. The transition was made to the KTX-Sancheon which has similar car-body and bogie systems with roughly half the total length (193.15 m). The configuration and numerical model discretization of the prototype train model used in this study is shown in Figure 2.4.

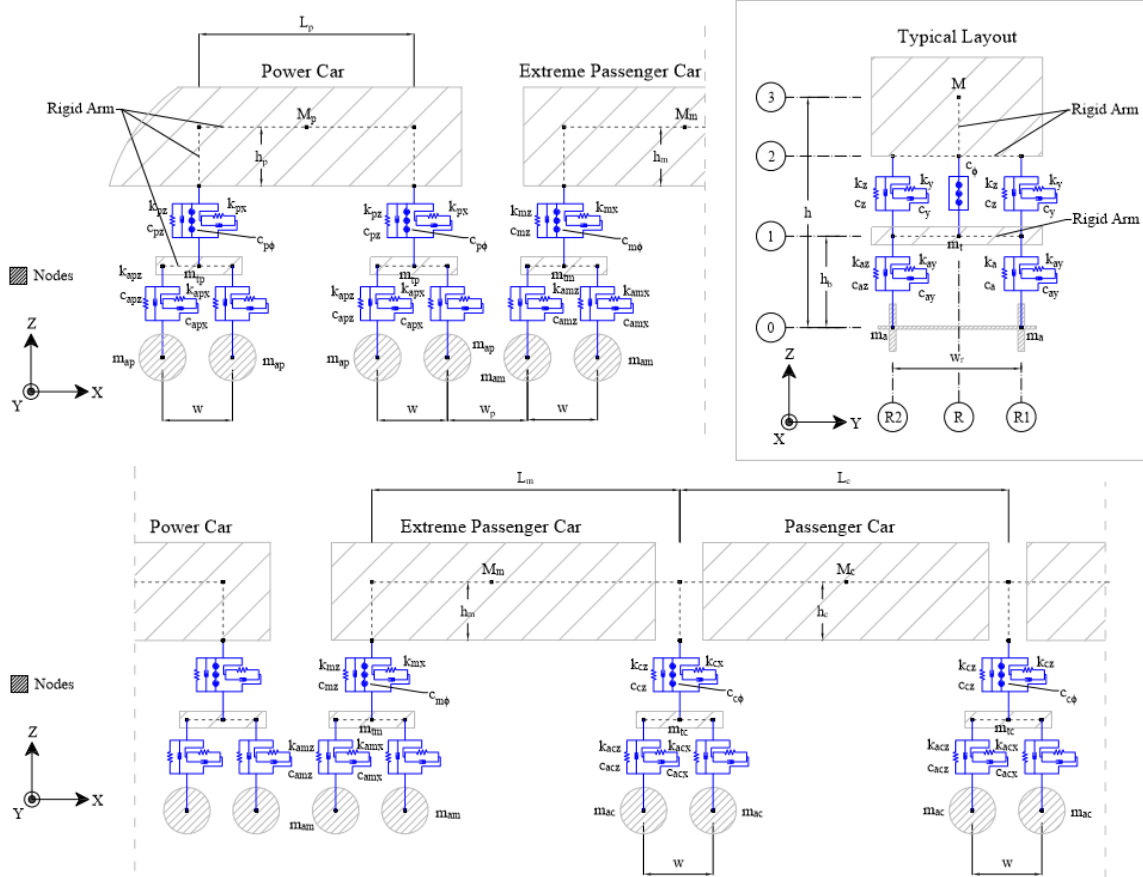


Figure 2.4. Schematic drawing for the numerical modeling of train system (Top: Cross-section, Bot: Elevation).

2.2.2.1. TRAIN SYSTEM MODEL GEOMETRY

Before defining the train nodes, lateral and vertical distances for the general location and geometric design of the train system were predefined to simplify the modeling process and allow for easy modification when necessary. As mentioned before, the track system of the prototype HSR bridge selected is a double track, which means there is a right (R) and left (L) track relative to the center of the bridge. From here onwards the right and left tracks will be referred to as track 1 and 2, respectively. Train dimensions retrieved from the reference study by Kwark et al. (Kwark et al. 2004) were used to define the train nodes. The train axle wheels are 3 m apart in the x-direction (w) and 2 m apart in the y-direction (w_r), so the rails for track system 1 were defined as R1 and R2 and are 1 m to the right and left of the track center line, respectively. Similarly, the rails for track system 2 were defined as R3 and R4. The lateral lengths of the power car (L_p), extreme passenger car (L_m), and intermediate passenger car (L_c) were defined respectively as 14.0 m, 18.7 m, 18.7 m, as well as the total length of the bridge system (L_T) as 193.15 m. The distance between the axle wheels of the power car and extreme passenger car is 3.275 m (w_p) (Kwark et al. 2004).

Various height parameters for the train system were also predefined. The rail height (h_r) was defined as 16.59 m, which is the sum of the column height (13.5 m) and girder depth (3.09 m). The



height of centroid for the bogies (h_b) were defined as 0.56 m and the height of centroid for the power and passenger car-bodies (h) were defined as 1.72 m and 1.627 m, respectively. These values were retrieved from a study by Song et al. (2003) who similarly modeled a Korean high-speed train assumed to be the KTX-I based on the dynamic properties of the mass constituent elements. The vertical distance between the bottom of the car-body and center-of-mass of the power car (h_p), extreme passenger car (h_m), and intermediate passenger car (h_c) were defined respectively as 0.605 m, 0.420 m, and 0.508 m. These values were taken from the reference study by Kwark et al. (Kwark et al. 2004). To expedite the process of shifting the train system along the length of the bridge, all train nodes were defined with an initial variable (x), which is the x-coordinate of the last wheel assuming the train is moving in the positive x-direction. The value (x) is adjusted depending on the load case being analyzed. A summary of all the parameters used for the train system is shown in Table 2.2.

Table 2.2. Dynamic Characteristics of Train Model.

Property	Power Car	Extreme Passenger Car	Intermediate Passenger Car
Mass of car-body (kg) [M]	54960	26000	26000
Primary sprung mass per bogie (kg) [m_t]	2420	2514	3050
Unsprung mass per axle (kg) [m_a]	2050	2050	2000
Primary stiffness per axle box (kN/m) [k_x, k_y, k_z]	40000, 9000, 1250	40000, 9000, 1250	55000, 11000, 800
Secondary stiffness per bogie side (kN/m) [k_{ax}, k_{ay}, k_{az}]	303, 303, 1270	100, 150, 370	100, 170, 303
Primary damper per axle box (kN-s/m) [c_x, c_y, c_z, c_ϕ]	0, 0, 10, 4230	0, 0, 10, 4230	0, 0, 6, 240
Secondary damper per bogie side (kN/m) [c_{ax}, c_{ay}, c_{az}]	0, 100, 20	0, 30, 20	0, 0, 0
Moment of inertia of car-body ($Mg-m^2$) [I_x, I_y, I_z]	59.4, 1132.8, 1112.9	33.94, 971.81, 971.81	33.94, 971.81, 971.81
Moment of inertia of bogie ($Mg-m^2$) [I_{tx}, I_{ty}, I_{tz}]	1.645, 2.593, 3.068	2.07, 3.26, 3.86	2.03, 3.20, 3.79
Moment of inertia of wheel ($Mg-m^2$) [I_{ax}, I_{ay}, I_{az}]	1.03, 0.0008, 1.03	1.03, 0.0008, 1.03	1.03, 0.0008, 1.03
Length of car-body (m) [L_p, L_m, L_c]	14.0	18.7	18.7
Height of centroid (m) [h, h_b]	1.72, 0.56	1.627, 0.56	1.627, 0.56
Height from secondary suspension arm to centroid (m) [h_p, h_m, h_c]	0.605	0.420	0.508



2.2.2.2. TRAIN SYSTEM NODES

Train nodes are created by defining the parameters specified for the node command. For large scale structural models for an OpenSees model to be filled with thousands of nodes, which can be very confusing if the node tags (NodeTags) are not organized. Since this study is modeling the train system running on track 1, the train node tags were organized where any tag starting with a 7 specified an alignment on the right side of the train over R1 (rail 1), an 8 specified an alignment on the left side of the train over R2 (rail 2), and a 6 specified an alignment on the centerline of track 1 (R). The second value of the node tag specifies the vertical grid of the train system as can be seen in the train model schematic (Figure 2.4). The value 0 is for the wheel nodes, 1 is for the bogie nodes, 2 is for the primary suspension nodes, and 3 is for the car-body nodes. The second to last number in the node tag specifies the bogie that the wheel, bogie, or suspension node is associated with, and the last number further specifies the location of the node within axle (1 or 2), bogie (1 to 3), or suspension system (1 to 3). For example, NodeTag 70042 designates the node for wheel 2 on the right side of bogie 4, and NodeTag 71052 designates the node for bogie 5's center node. This trend is not followed for the car bodies. Instead, the last digit of the car-body node tags ranges from 1 to 23. Each car-body is constituted by three nodes and car-bodies for the articulated system share a node as can be seen in Figure 2.4.

All coordinates are defined using the predefined parameters as discussed in Section 3.2.2.1 above. This allows for simple adjustment of the train dimensions in the case of a parametric study or adjustment to a potential design. For the intermediate passenger cars, a value "n" was set to represent the respective number of the 6 intermediate passenger cars. A value of 1 was set for the first intermediate passenger car which was used to define the x-coordinates of the nodes, and each successive intermediate passenger car nodes were defined by increasing the n value by 1. The variable "x" previously defined and shown in Figure B-1 is included in the x-coordinates of every train node to shift the location of the entire train system along the length of the bridge. The z-coordinates were defined with the predefined train system heights as shown in Figure 2.4. Wheel nodes were modeled at the same height as rail nodes under the assumption of perfect contact and the height of the bogie nodes were modeled as the sum of the rail height and bogie height relative to the rail. The z-coordinate of car-bodies were defined as the sum of the height of their center-of-mass (h) assumed in Section 3.3.2.1 and the height of the rail (h_r). and the top node of the secondary suspension system as the sum of car-body height (h) and the height of the rail (h_r), minus the respective cars vertical distance between the car-body center of mass to the bottom of the car-body.

2.2.2.3. TRAIN SYSTEM RIGID CONNECTIONS

The car-body and bogie are modeled as elastic beam-column elements with exceedingly stiff properties. The cross-sectional area, Young's modulus, shear modulus, torsional moment of inertia of the cross-section, and second moment of area about the local z and y-axis were assigned exceptionally large values to create a rigid element. Exceptionally stiff elements can potentially cause convergence issues depending on the type of convergence test type for analysis, so the values



should be defined accordingly. Since the KTX-Sancheon has an articulated bogie system, the passenger cars act as a coupled unit. The car-bodies for the extreme and intermediate passenger cars are modeled as rigid beam-column elements in series; however, the power cars are disconnected from the rest of the system.

2.2.2.4. TRAIN SYSTEM SUSPENSIONS

Flexibility is provided in the train system through the primary suspensions system between the axles and bogies, and the secondary suspension system between the bogies and car-bodies. The primary and secondary suspension system of the train were modeled using the twoNodeLink link element command in OpenSees. This command allows the user to construct a zero or non-zero length element defined by two nodes and apply material behavior to any transverse or rotational DOFs for a three-dimensional model. Uniaxial elastic materials were used to model the stiffness in the translational DOFs, and uniaxial viscous damper materials were used to model the vertical damping within the suspension system. Stiffness and damping coefficients for the suspension system of the power car, extreme passenger car, and intermediate passenger car were defined as given in the reference study (Kwark et al. 2004). The parallel material command was used to combine the stiffness and damping material in the z-direction to a single material. These materials were then used as the material parameters for the two-node link elements. The i-nodes shown are the bogie nodes and the j-nodes are the axle wheel nodes. The materials defined were applied in their respective directions and the orient command was used to manually instruct OpenSees of the element vector components. Since the primary suspension system only applies stiffness in the three translational DOFs, the equalDOF command was used to constrain the remaining DOFs between the bogie and axle nodes.

Similar process was performed for the secondary suspension systems; however, damping for the z-rotational DOF was also applied in addition to any translational. As shown in the train model schematic in cross-section of the train model in Figure 2.4, the secondary suspension system has three layers: left, middle, and right. The left and right layers supply stiffness and damping in the translational DOFs and the middle layer supplies damping in the z-rotational DOF. Due to this DOF not having any stiffness, the DOF must be constrained for the stability of the model. However, if the displacement between the two-nodes constituting the middle layer of the secondary suspension system were constrained using the equalDOF command, the z-rotational damping would not activate due to the lack of displacement (x). Therefore, a relatively small stiffness value (1 kN/m) was applied in the z-rotational DOF to allow for the activation of the damping, and the rest of the DOFs were constrained using the equalDOF command.

2.2.2.5. TRAIN SYSTEM MASSES

The train masses were modeled using the values given in the reference study (Kwark et al. 2004), included in Table 2.3. Since the extreme passenger car for the KTX-Sancheon is not motorized, unlike the KTX-I in the reference study, the translational mass and inertial mass values for the intermediate passenger car were used for the extreme passenger car as well. The masses were defined at the center-of-mass nodes for each car-body and bogie. The masses for the wheels are defined at every wheel node. The inertial masses were used to define the rotational nodal masses.



Table 2.3. Masses for Track-Bridge System.

	Mass (Mg/node)	Moment of Inertia 1 (Mg-m ²)	Moment of Inertia 2 (Mg-m ²)	Moment of Inertia 3 (Mg-m ²)
Girder	63.7359	159.1817	61.1692	189.1868
Column	7.9940	27.2587	11.7515	23.8342
Footing	629.7408	7859.6900	7859.6900	14122.9870
Rail	0.1693	0.0025	0.1459	0.1446
Track Plate	3.5878	1.9561	3.0640	4.9961
Base Plate	3.9466	2.8739	3.3691	6.2193

2.2.3. TRAIN SYSTEM MODEL

The track system comprises of rails, track plates, base plates, and the connection layers in between these components. The rails, track plates, and base plates were modeled as elastic-BeamColumn elements and the connection layers were modeled as zeroLength elements. The rails, track plates, and base plates were discretized into equal intervals of 3.195 m and the connection layers were modeled at the end nodes of each interval. The train-track interaction was modeled by including and connecting the train wheel nodes as a member of the series of nodes creating the rail elements. This directly transfers the train loads to the track system, which then transfers the loads down to the bridge system through rigid arms connecting the track system to the bridge girder. The bridge girder was also discretized into equal increments of 3.195 m, which allowed for the track-bridge interaction to occur at an equal distribution along the entirety of the bridge length. A general schematic of the track system is shown in Figure 2.5 and Figure 2.6. The steps taken to model the track system nodes, elements, and masses are further discussed in detail in this section.

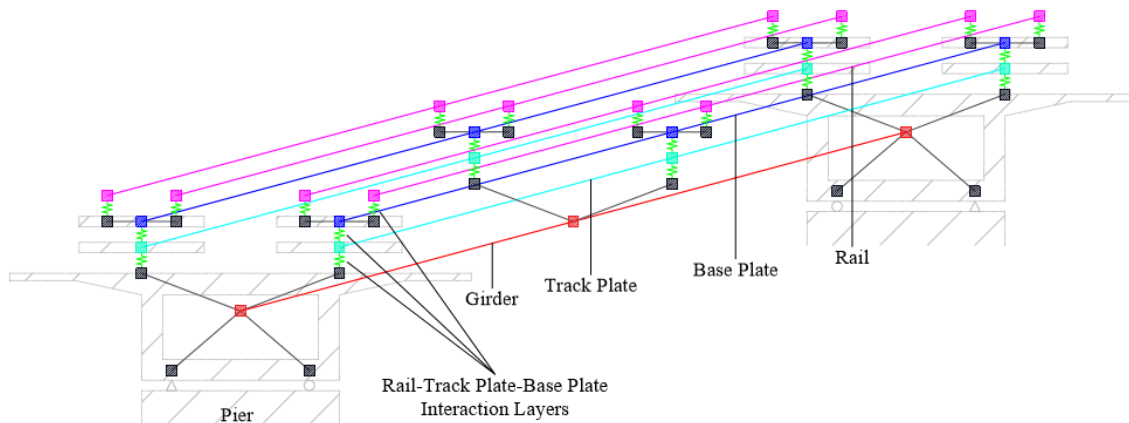


Figure 2.5. Schematic of track system.

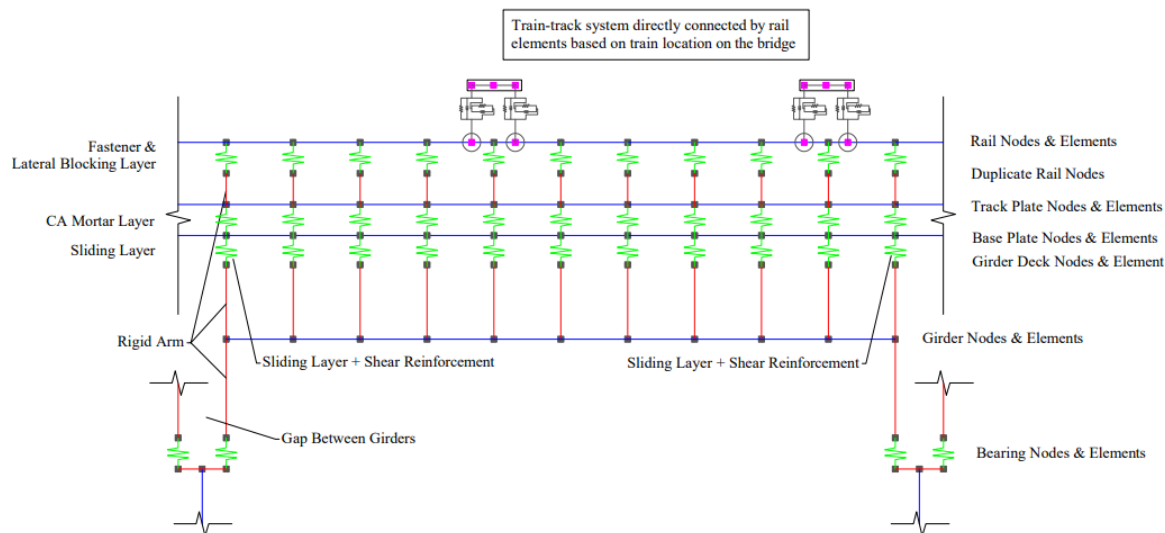


Figure 2.6. Schematic of track-bridge system.

2.2.3.1. TRACK SYSTEM ELASTIC ELEMENTS

The rails, track plate, and base plate were modeled as linear elastic beam-column elements because they are all designed to remain elastic as capacity protected elements. The location of the track plate and base plate nodes are the same, and rail nodes are located to the right and left of the track plate/base plate nodes by half the transverse train wheel spacing, defined earlier as R1 and R2 for track 1 and L1 and L2 for track 2, respectively. The elements were assigned cross section parameters as given in the study by Li et al. (Li et al. 2020). The rail, track plate, and base plate elements span the entirety of the bridge length.

To connect the train system to the track system, wheel nodes of the train were connected to neighboring rail nodes using the same linear elastic beam-column elements used for the rails. Since the train was placed on track 1 consisting of rails 1 and 2, the wheel nodes were modeled at the same y and z-coordinates as the rail nodes. The sequential order of the wheel nodes and rail nodes were organized offline and defined in OpenSees accordingly. This was done under the assumption that the train wheels are always in contact with the rails, which is a common assumption.

2.2.3.2. TRACK SYSTEM CONNECTION LAYERS

Zero-length elements were used to simulate the nonlinear behavior of the sliding layer, CA layer, shear reinforcement, lateral blocking, and fasteners. The nonlinear material behavior was assigned to the zero-length elements using the Steel01 material in OpenSees. The yield strengths were assigned as given by Li et al. (Li et al. 2020) and the initial elastic tangent was found by a quotient of the yield strength and relative displacement. The strain hardening ratio was assigned a value of zero to mirror the perfectly elastic-plastic behavioral graph from the reference study. Figure 2.7 first shows the generalized elastic-plastic behavior along with the parameters of the different zero-length connection elements in the track-bridge system as adopted from Li et al. (Li



et al. 2020). Next, dedicated plots were generated to demonstrate the behavior of five of those connection components in track systems and shown in Figure 2.8. The CA mortar layer was modeled between the track plate and base plate (Figure B-26), and the sliding layer was modeled between the base plate and rigid arm connecting the track system to the bridge girder. The fasteners, CA mortar layer, and sliding layer allow for longitudinal slippery relative to the bridge length. Multi-point constraints were used to constrain the remaining DOFs of the connection layer nodes that stiffness was not applied to through zero-length elements. For example, stiffness was applied in the longitudinal direction for the sliding layer to allow for movement based on the behavior of the material, so the equalDOF command was used to constrain the remaining 5 DOFs.

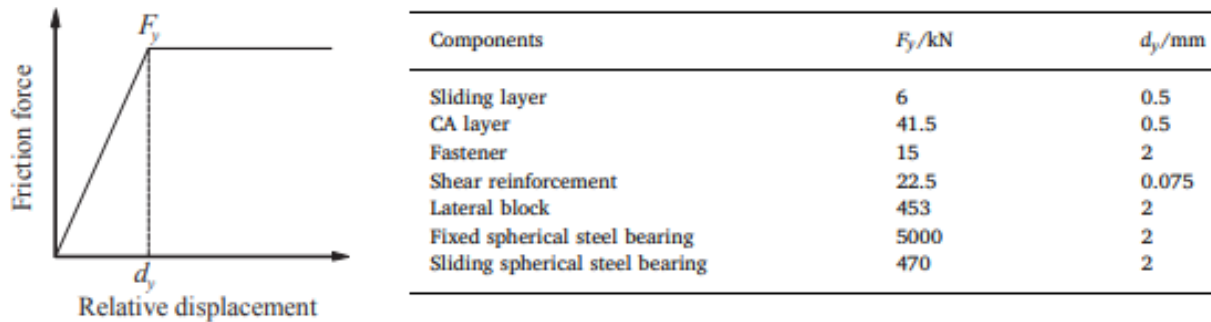


Figure 2.7. Parameters of zero-length connection elements in the track-bridge system as adopted from Li et al. (Li et al. 2020).

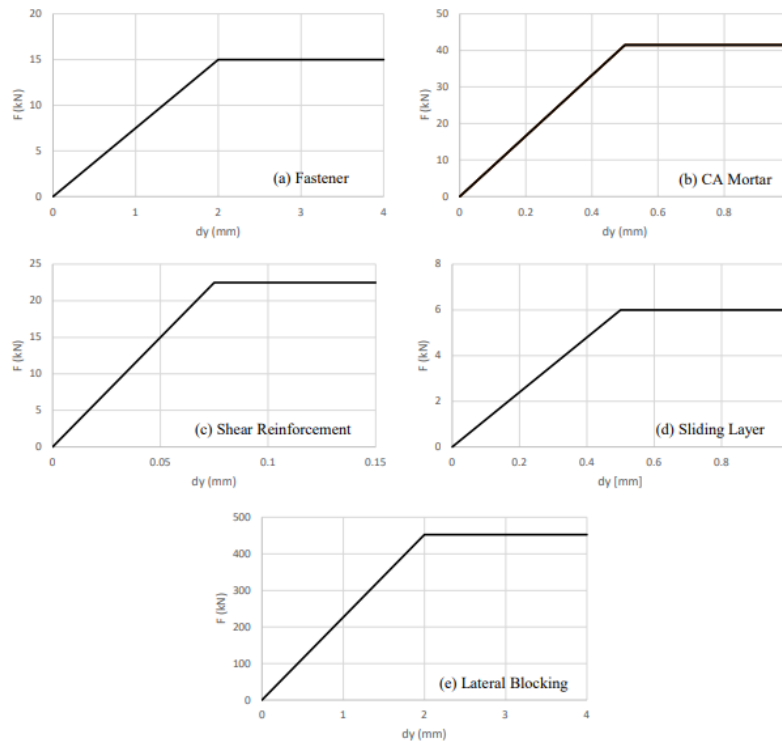


Figure 2.8. Force-deformation behavior of track system connection layers: (a) Fastener, (b) CA mortar, (c) Shear reinforcement, (d) Sliding layer, and (e) Lateral blocking



2.2.3.3. TRACK SYSTEM RIGID CONNECTIONS

Rigid elements were used in the track system to connect the track plate nodes to the rails. Specifically, the rigid arms branch out from each track plate node to duplicate rail nodes that were not used to model the rail elements. The rigid section properties to model rigid arms out of elastic beam-column elements were kept the same as what was used for the train system rigid bodies. Rigid arms were modeled at 3.195 m intervals for both tracks 1 and 2, which is the same intervals as the track system nodes. The location of the rigid arms can be seen in Figure 2.9.

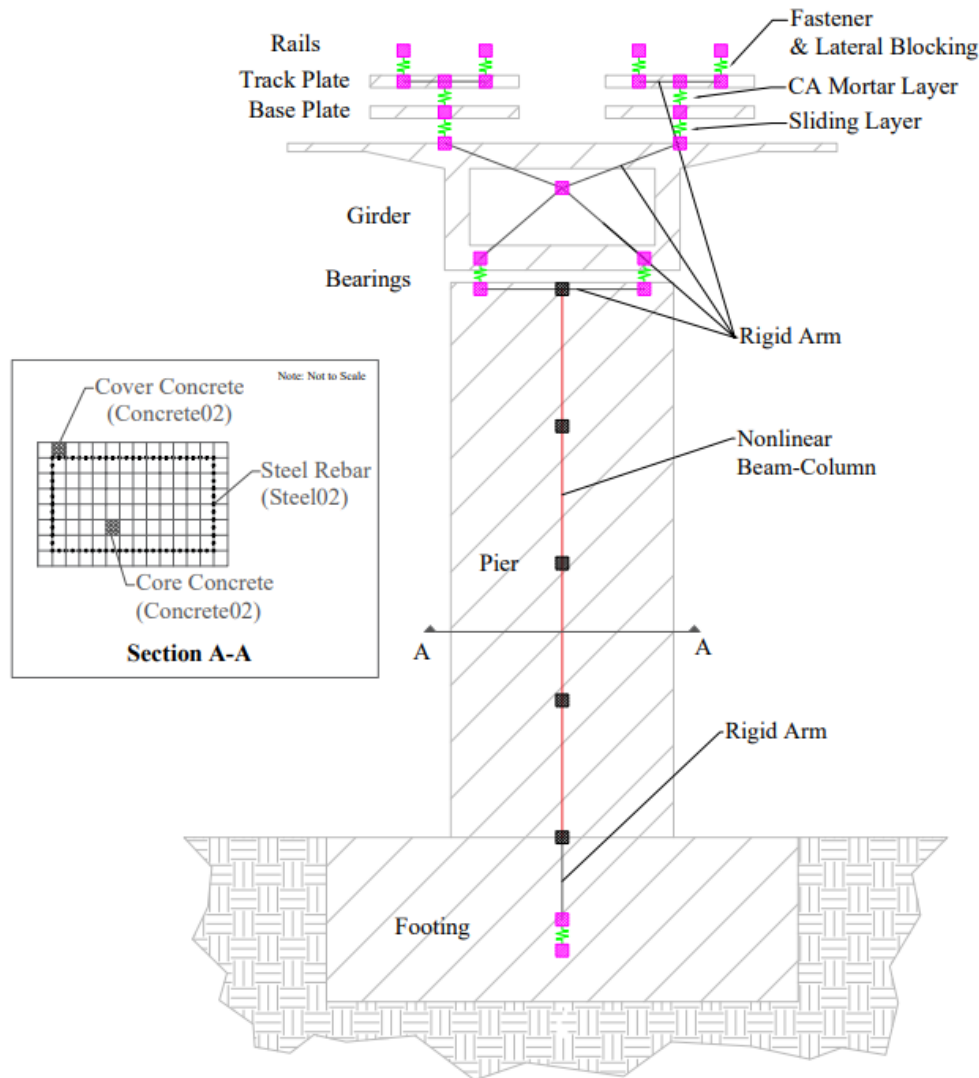


Figure 2.9. Schematic of track-bridge system.

2.2.3.4. TRACK SYSTEM RIGID MASSES

The masses for the rails, track plates, and base plates were assumed using approximate densities of steel and concrete. The steel rails were assumed to have a density of $7,700 \text{ kg/m}^3$, and the concrete track plate and base plate were assumed to have a density of $2,400 \text{ kg/m}^3$. These are



very generic values and accurate densities should be utilized to accurately model the dynamic performance of HSR systems because the mass matrix is one of the key components of solving the equation-of-motion of the model. Mass per node was found by dividing the product of the given cross-sectional area and the length of the bridge by the number of nodes constituting the entire length (110 nodes). General mass moment of inertia equations for rectangular sections were used to solve for the moment of inertia in the three rotational DOFs. The masses used for the track system in this study is shown in Table 2.3. The mass per node was used for the nodal mass value in the translational DOFs and the inertial masses were used for the rotational DOFs.

2.2.4. BRIDGE SYSTEM MODEL

The bridge system comprises of girders, bearings, pier columns, and footings. Girders were modeled as elastic beam-column elements, and bearings were modeled as zero-length elements. Pier columns were modeled as displacement based elastoplastic fiber elements and columns footings were modeled as rigid elements. Rigid arms were used to connect each bridge component to one another as illustrated in the track-bridge system schematic shown in Figure 2.9.

2.2.4.1. TRAIN SYSTEM GIRDER

The prestressed concrete box-girder bridge is designed to be elastic, i.e., capacity protected component for seismic considerations, so linear elastic beam-column elements with equivalent section characteristics were used to model the superstructure. Each span was discretized into 10 equivalent lengths of 3.195 m by creating 11 nodes per girder span. A 0.05 m gap was created between each bridge girder span to simulate the isolated movement allowed to each girder span by four steel bearings, two fixed and two sliding. The cross-sectional area, Young's modulus, shear modulus, torsional moment of inertia of the cross-section, and second moment of area about the local z and y-axis were assigned the values given by Li et al. (Li et al. 2020) and shown in Table 3-4. To simulate the process of bridge design, the Young's Modulus was decreased from 3.45×10^7 kN/m² to 2.45×10^7 kN/m² and the moment of inertia values were reduced by 30% to account for the reduction in concrete stiffness due to cracking.

Table 2.4. Section parameters of elastic beam elements in track-bridge system as adopted from Li et al. (Li et al. 2020).

	Sectional area/m ²	Elastic modulus /kN/m ²	Shear modulus /kN/m ²	Torque /kN m	Inertia moment 1/m ⁴	Inertia moment 2 /m ⁴
Main girder	9.06	3.45×10^7	1.44×10^7	2.26×10^1	1.10×10^1	9.48×10^1
Base plate	5.61×10^{-1}	3.00×10^7	1.25×10^7	6.74×10^{-3}	1.69×10^{-3}	4.06×10^{-1}
Track plate	5.10×10^{-1}	3.55×10^7	1.48×10^7	6.80×10^{-3}	1.70×10^{-3}	2.76×10^{-1}
Rail	7.75×10^{-3}	2.06×10^8	8.05×10^6	2.00×10^{-6}	3.20×10^{-5}	5.00×10^{-6}

2.2.4.2. BRIDGE SYSTEM BEARINGS

The spherical steel bearings were modeled using zero-length elements. To use zero-length elements, the OpenSees user must create two nodes with the same coordinates, hence the zero-length. Since the bearings are located at the ends of each bridge span, two-sets of nodes were created accordingly. The fixed and sliding bearings were assumed to be 4 m apart, based on the box-girder dimensions, in the direction transverse to the bridge at the top of the 13.5 m tall pier columns. One set of the bearing nodes were used to connect the bearing system to the bridge



girder, and the other set of nodes were used to connect the bearings to the top of the pier columns, both through rigid arms.

The OpenSees material command *Steel01* was used to define the bilinear behavior of the steel bearings within the zero-length elements. The required parameters for the zero-length elements for the steel bearings are shown in Figure 2.7. The yield strength was defined as given by the reference study in Figure 2.7 with a value of 5000 kN for the fixed bearing and 470 kN for the sliding bearing, and the elastic tangent or slope of the elastic region was found by a quotient of the yield strength and relative displacement also given in Figure 2.7. As previously mentioned, the strain-hardening ratio was set as 0 and the uniaxial material was applied into directions 1 and 2 to apply stiffness in the lateral translational DOFs. The behavior of the fixed and sliding bearing is shown in Figure 2.10. The fixed and sliding bearings were alternated as shown in Figure 2.11 to mirror the design of the actual bridge.

As previously mentioned, stiffness was only applied in the longitudinal and transverse DOFs, so the vertical DOF and the three rotational DOFs were constrained for structural stability. The high stiffness value for the fixed bearing idealizes the resistance it provides to constrain movement and the low value for the sliding bearing idealizes the slight resistance it provides despite allowing movement.

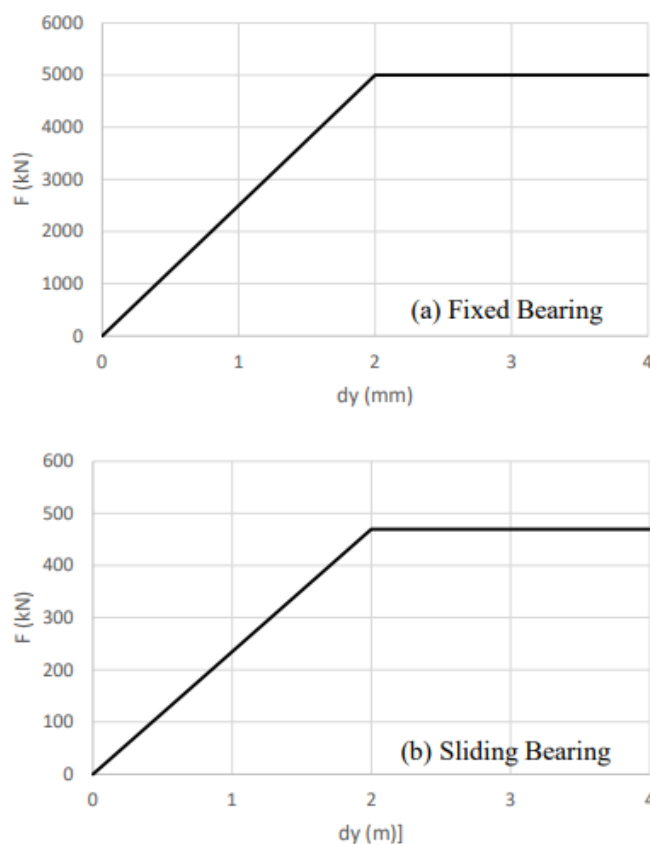


Figure 2.10. Force-deformation behavior of bridge bearings: (a) Fixed bearing, (b) Sliding bearing.

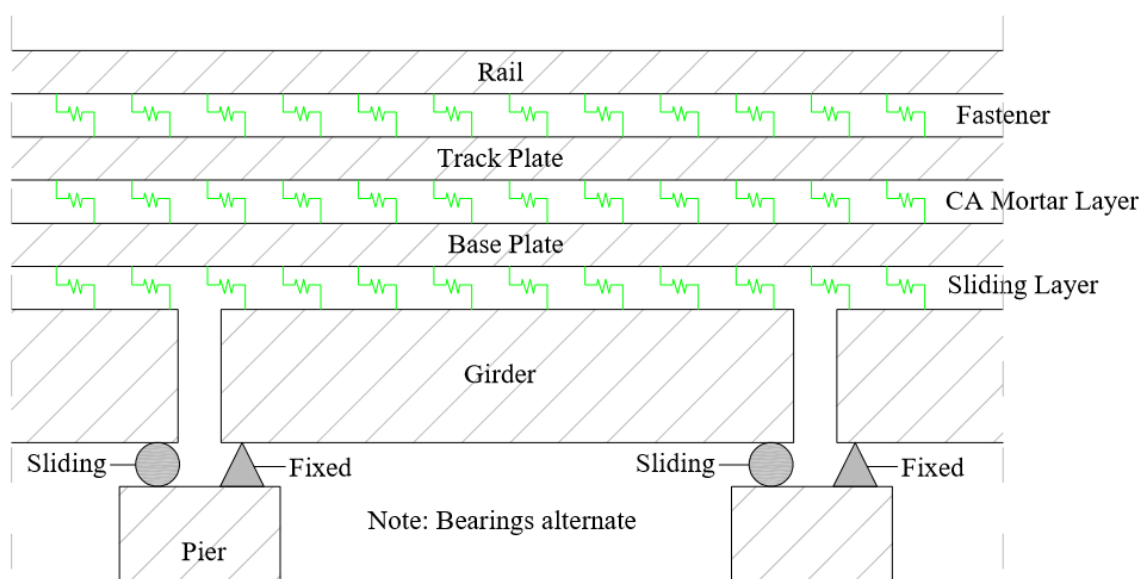


Figure 2.11. Finite element model of bridge.

2.2.4.3. BRIDGE SYSTEM PIER COLUMNS

Materials for the pier column cross-section were defined using uniaxial materials available within OpenSees and material strengths were input as parameters. The core concrete, cover concrete, and reinforcing steel strength assumptions were adopted from a sample code provided by the OpenSeesWiki (Gregory L. Fenves et al. 2020) since the design guideline for the selected prototype HSR bridge used herein did not provide sufficient information on specific material specifications for the bridge columns. The cover and core concrete were modeled using the Concrete02 material and the longitudinal reinforcement was modeled using the Steel02 material in OpenSees; a typical modeling practice for bridge elements that has been adopted in many of the reviewed studies such as Li and Conte (Li and Conte 2016). For the Steel02 command, the R0, cR1, and cR2 parameters were defined as 15, 0.925, and 0.15, respectively, as recommended for general reinforcing bar by the OpenSeesWiki.

The pier cross-section was created using the fiber section command. The cover and core concrete were defined within the section using the patch rect command to generate fibers over a rectangular cross-sectional area. The reinforcing steel was defined using layer straight commands to generate fibers along a straight line for the four sides of the rectangular cross-section. The material tag (matTag) for these commands reflects what was defined for the cover, core, and reinforcing steel materials.

The geometry of cross-section design, as well as the coordinates required in the command parameters to create the cross-section were predefined. A reinforcement ratio of 1.30% was assumed for the cross-section and this led to a preliminary design of 176- #11 bars, split into 60 bars on the long face and 28 bars on the short face of the cross-section. Transverse reinforcement was assumed as #4 bars and a clear cover of 0.04 m was also assumed. The design used for the cross-section does not reflect the actual design of the pier columns, but since the details are unknown,



a general design was done based on engineering judgement. The design specified in the section Fiber command was then aggregated into a uniaxial elastic material section using the section Aggregator command to create a single section force-deformation model. The torsion force-deformation (T) was selected as the force-deformation quantity parameter to be modeled by the section object.

The rectangular bridge pier columns were modeled as a series of four three-dimensional displacement based elastoplastic fiber elements using the dispBeamColumn command with the nonlinear fiber cross-section that was defined. Each pier was constituted by five nodes with equal 3.375 m intervals with five integration points each. Integration of fiber characteristics over the pier cross-section allowed for the obtainment of nonlinear section characteristics.

2.2.4.4. BRIDGE SYSTEM COLUMN FOOTINGS AND SOIL

Column footing dimensions of the prototype bridge selected were not explicitly noted in the reference study, so generic dimensions of 4 m for the depth and 11 m for the width were assumed. The nodes were defined at -2 m to create nodes at the centroid of the footings. The column footings were modeled as rigid elements via the same method for all other rigid elements to connect the column base nodes to the footing nodes.

Due to the focus of the study being the dynamic interactions between the train-track-bridge systems, a simplistic method was used to model the interaction between the bridge and soil. Since California is projected to be the home of the largest HSR system in the United States, soil spring constants from a study by Abbasi (2018) were used to simulate the general soil properties of California. Since multi-column box-girder bridges in California typically have the pinned connection details in the foundation, there are no rotational stiffness defined at the column footings. Abbasi (Abbasi 2018) considered a wide range of soil profiles and foundation systems over the state of California and determined the stiffness of translational springs to be 115 MN/m. However, adjustments were made to accommodate the single column bent design of the bridge piers. Single column bents typically utilize fixed-base connections to provide stability to the cantilevered system. Accordingly, the footing nodes were fixed in the non-translational DOFs and the foundation nodes were fixed in all 6 DOFs to create a base for the entire model.

The structure-soil interaction was simplified in-part due to the lack of information regarding the soil spring constants required to model the pile-soil interaction and the focus of the study being the train-track-structure interaction. If this information is available, a sophisticated soil-structure interaction model is recommended by explicitly modeling the piles as displacement based elastoplastic fiber elements, as done by Li et al. (Li et al. 2020) and Li and Conte (Li and Conte 2016).

2.2.4.5. BRIDGE SYSTEM RIGID CONNECTIONS

Rigid elements are used in the bridge system to connect the bridge girder, bearing, pier column, and footing to one another. For the model in-place, the track system is connected to the bridge girder through two diagonal arms at an interval of 3.195 m, along the entire bridge length. Additionally, two diagonal rigid arms connected the bridge girder to the steel bearings isolating the bridge girder from the pier columns, meaning the two nodes defining the ends of each bridge



girder span had a total of four rigid arms. The bearings are connected to the pier columns through two horizontal arms in the y-direction at the top of the pier columns, and the column footings are idealized as a rigid arm. The location of rigid arms is shown in the track-bridge system schematic in Figure 2.9. The same rigid section properties were used as the rigid arms in the train and track system.

2.2.4.6. BRIDGE SYSTEM MASSES

For the dynamic equation of motion, masses for the concrete deck, pier column, and footing can be assumed using a standard density of $2,400 \text{ kg/m}^3$. General mass moment of inertia equations for rectangular sections were used to solve for the very approximate mass moment of inertia in the three rotational DOFs. The masses of the bridge girder were distributed along the 10 spans, consisting of 11 nodes each. The masses of each pier column were distributed along the five nodes constituting the entire column. The masses were applied at the center-of-mass node for each footing. The masses for the bridge system in this study is shown in Table 2.3 as previously mentioned.

3. CONCLUDING REMARKS

The overall goal of this study is to synthesize the existing and ongoing efforts for HSR bridge systems through extensive review and understand the approaches to provide potential solutions to new design and construction. A focus is given to the modeling and numerical simulation techniques for various HSR systems and identify common modeling practices. The work presented in this study is critical and timely as the implementation of HSR as a major mode of transportation in the United States is coming into fruition. Due to the recent advances in HSR research, national studies regarding this topic are still very limited and heavily rely on the publications from researchers abroad in Europe and East Asia where HSR systems are widely used as a major method of transportation. Sub-systems of HSR have evolved over the years as technological advancements continue to improve the safety and efficiency of HSR. The extensive literature search presented in this study synthesizes the modeling methods that have been used by national and international researchers to idealize variety of train, track, and bridge systems. Future researchers can access this study to understand how specific HSR sub-systems are modeled and can pursue the publications referenced within this study for further details since.

Modeling techniques from literature published by researchers around the world are analyzed and discussed to understand the dynamics of train-track-bridge interactions. Studies modeling different types of HSR train systems, track systems, and bridge systems were explicitly researched to offer a comprehensive literature search that will allow the reader to gain insight on the modeling techniques of various HSR systems. This study identifies critical modeling features needed to develop a detailed numerical model, based on synthesized literature, that can capture HSR train-track-structure interaction under service and extreme loads including seismic excitations. A prototype train, track, and bridge system are selected based on available information that can be incorporated into a prototype model. The selections were then used to create a detailed HSR model in OpenSees using the modeling techniques synthesized in the extensive literature search



to achieve the second objective. The model is then created to demonstrate the functionality of the modeling techniques. This study provides a step-by-step walk-through of the processes of modeling a prototype HSR system including the train-track-bridge system in detail. This guide will allow future students and researchers with minimal experience in numerical modeling or modeling in OpenSees to formulate their own HSR model. This guide can also be of benefit to researchers or designers who may need some guidance, as existing publications regarding this topic focus mainly on the analysis and results rather than the specific methods used to model each sub-system.

For completeness, a statement on the validities and limitations of this study are presented here and discussed to provide points of future recommendations and improvements. Due to the recent emphasis on implementing HSR systems as a mode of transportation in the US, the literature available is heavily limited to a few national studies and foreign studies that have been translated to English and published to journals. This results in limitation of reference studies that can be researched for the purpose of understanding the methods of numerical modeling of HSR systems.

Another issue is the validity of the prototype model analysis results due to the lack of available design information regarding the prototype train, track, or bridge system that have been selected from the reference studies. This is mainly due to the limitation of content that can be included in such journal papers which could lead to the omission of detail that is not the emphasis of the respective study. A design assumption example being the cross-sectional design and strength of concrete and reinforcing steel of the pier columns for the prototype bridge from the Beijing to Xuzhou section of the Beijing-Shanghai high-speed railway. Although the cross-sectional area and height of the pier columns were specified, the reinforcement layout and strength design were omitted so generic assumptions were made regarding reinforcement ratio and strength of core concrete.

The train-track-structure interaction was the focus of the modeling. Accordingly, soil-structure interaction was simplified to a few springs between the column bases and the fixed boundaries of the model. Future studies should elaborate on the modeling of soil-structure interaction by creating a sophisticated footing model with pile-soil interaction and abutments at bridge ends. In addition, elements were not discretized as precisely as recommended for a study focusing on analysis results, since the focus is to demonstrate the process of modeling and analyzing a prototype model. The prototype HSR bridge model in place is a primitive design combining a train system from Korea, a track-bridge system from China, and general soil properties from California under the assumption that they are all compatible for the sake of demonstrating a model.

A proper seismic analysis of any structural system requires a design guideline and code that acts a standard for the performance of the structural design. Since there is no such standards in-place for HSR bridges in the US as of yet, the performance of the prototype HSR bridge was based on engineering judgement and preexisting knowledge based on highway bridges. The modeling strategy presented in this article may help develop a formal design guideline and code.



4. REFERENCES

- Abbasi, M. (2018). "Seismic Vulnerability Assessment of As-Built and Retrofitted Multi-Frame Box-Girder Bridges." *University of Nevada, Reno*.
- Alfach, M. T. (2019). "Reinforcement of the seismic interaction of soil-damaged piles-bridge by using micropiles." *Jordan Journal of Civil Engineering, University of Wolverhampton, UK*.
- American Galvanizers Association. (2012). "Galvanized Steel Pile Cap for Micropile Transmission Tower Foundations." *galvanizeit.org, San Diego, California*.
- Andersson, A., and Karoumi, R. (2015). "Dynamics of railway bridges, analysis and verification by field tests." *MATEC Web of Conferences, (G. Feltrin, ed.), 24(January), 12*.
- California High-speed Rail Authority. (2015). *California High-Speed Rail Authority Request for Proposals for Design-Build Services for Construction Package 4 Book III , Part A . 1 Design Criteria Manual*.
- California High-Speed Rail Authority. (2019). *California High-Speed Train Project Design Criteria, Rev. 3. Sacramento, CA*.
- Chin, C.-T., and Chen, J.-R. (2007). "Foundation engineering practice in Taiwan – High Speed Rail Experiences." *Proc., Seminar on the State-of-the-Practice of Geotechnical Engineering in Taiwan and Hong Kong, 28–51*.
- Combault, J. (2013). "Design and construction of segmental bridges for high speed rail." *Aspire, 7(4), 18–21*.
- Dong Kang, K., and Suh, S. D. (2003). "Experience with the Precast Span Method on the Korean High-Speed Rail Project." *Transportation Research Record: Journal of the Transportation Research Board, 1825(1), 15–21*.
- Evangelista, L., and Vedova, M. (2009). "The Italian high speed network: Design and construction of the reinforced concrete bridges." *Bridges for High-speed Railways, R. Calçada, R. Delgado, and A. C. e Matos, eds., CRC Press, 47–59*.
- Gingery, J., O'Neill, B., Hilton, B., Jong, K., and Winkle, H. Van. (2011). *Geotechnical Analysis and Design Guidelines*.
- Gregory L. Fenves et al. (2020). *OpenSeesWiki*.
- He, X., Wu, T., Zou, Y., Chen, Y. F., Guo, H., and Yu, Z. (2017). "Recent developments of high-speed railway bridges in China." *Structure and Infrastructure Engineering, 13(12), 1584–1595*.
- Herbst, T. . (1994). "The GEWI-PILE, a micropile for retrofitting, seismic upgrading and difficult installation." *International Conference on Design and Construction of Deep Foundations, Federal Highway Administration (FHWA), 913–930*.
- International Code Council. (2015). *International Building Code*.



- International Union of Railways. (2006). UIC Code Leaflet 776-1R - Loads to be considered in railway bridge design.*
- Janberg, N. (2020). "structurae.net." Structurae - The Largest Database for Civil and Structural Engineers.*
- Kang, C., Schneider, S., Wenner, M., and Marx, S. (2018). "Development of design and construction of high-speed railway bridges in Germany." Engineering Structures, 163(December 2017), 184–196.*
- Kim, M. (2014). "KTX-Sancheon."*
- Kimmerling, R. E. (2002). Geotechnical Engineering Circular No. 6 - Shallow Foundations. Seattle, Washington.*
- Kwark, J. W., Choi, E. S., Kim, Y. J., Kim, B. S., and Kim, S. I. (2004). "Dynamic behavior of two-span continuous concrete bridges under moving high-speed train." Computers & Structures, 82(4–5), 463–474.*
- Li, H., Yu, Z., Mao, J., and Jiang, L. (2020). "Nonlinear random seismic analysis of 3D high-speed railway track-bridge system based on OpenSEES." Structures, 24, 87–98.*
- Li, Y., and Conte, J. P. (2016). "Effects of seismic isolation on the seismic response of a California high-speed rail prototype bridge with soil-structure and track-structure interactions." Earthquake Engineering & Structural Dynamics, 45(15), 2415–2434.*
- Manterola, J., and Escamilla, M. (2014). "Steel and composite bridges for high speed rail: Advanced solutions for challenging designs." American Institute of Steel Construction (AISC) Symposium, Toronto, CA, 6.*
- Marx, S., and Schlaich, J. (2009). "Gestalten von Eisenbahnbrücken." Stahlbau, 78(3), 197–202.*
- Mason, J. A. (1993). CALTRANS full scale lateral load test of a driven pile foundation in soft bay mud. Sacramento, CA.*
- Minami, K., and Shimizu, K. (2011). "Design of Steel Bridges for Shinkansen, Japan, High-Speed Rail." Transportation Research Record: Journal of the Transportation Research Board, 2228(1), 131–138.*
- Momenzadeh, M., Nguyen, T., Lutz, P., Pokrywka, T., and Risen, C. (2013). "Seismic Retrofit of 92/280 I/C Foundations by Micropile Groups in San Francisco Bay Area, California." International Conference on Case Histories in Geotechnical Engineering, Missouri University of Science and Technology, Chicago, Illinois.*
- Muncke, M. (2008). "The effects on the interoperability of the European Railway Traffic of European Standards." Bridges for High-Speed Railways, R. Calçada, R. Delgado, and A. C. e Matos, eds., CRC Press, 15–22.*
- Parmantier, D. M., Armour, T. A., Perkins, B. J., and Sexton, J. A. (2004). "Foundation Seismic Retrofit of Boeing Field Control Tower." GeoSupport 2004, American Society of Civil Engineers, Reston, VA, 278–288.*



- Parsons Brinckerhoff. (2009). Design Guidelines for High-Speed Train Aerial Structures: 2.3.3 (Technical Memorandum).
- Pearlman, S. L., Wolosick, J. R., and Gronek, P. B. (1993). "Pin piles for seismic rehabilitation of bridges." the 10th International Bridge Conference, Pittsburgh.
- Rosignoli, M. (2016). "Full-Span Precasting of High-Speed Railway Bridges." Bridge Tech, *The Bridge Engineering eManuals*.
- Shu, S., and Muhunthan, B. (2010). Influence of Sand State on Network effect of Micropiles.
- Sobrino, J. (2008). "Bridges for the high speed railway lines in Spain. Design criteria and case studies." Bridges for High-Speed Railways, R. Calçada, R. Delgado, and A. C. e Matos, eds., CRC Press, 71–91.
- Song, M.-K., Noh, H.-C., and Choi, C.-K. (2003). "A new three-dimensional finite element analysis model of high-speed train–bridge interactions." Engineering Structures, 25(13), 1611–1626.
- Tai, J. C., Jang, D., Gaffney, H., and Flint, J. (2010). "Full Span Precast and Launching Construction in Taiwan's High Speed Rail Project." 2010 Joint Rail Conference, Volume 1, ASMEDC, 167–173.
- Tom Armour, Gronek, P., Keeley, J., and Sharma, S. (2000). Micropile Design and Construction Guidelines Implementation Manual Priority Technologies Program Project. Federal Way, WA.
- Yan, B., Dai, G. L., and Hu, N. (2015). "Recent development of design and construction of short span high-speed railway bridges in China." Engineering Structures, Elsevier Ltd, 100, 707–717.
- Zhou, Y. E., Drive, N. P., Valley, H., and Niu, B. (2012). "Considerations for Development - High-Speed Rail Bridge Design Standards." Proc., AREMA 2012 Annual Conference, Chicago, Illinois, 47.